DTP-93-66

Fermilab Library
0 1160 0036862 5

DTP/93/66
August 1993

42

Structure Functions and Small x Physics[1]

A.D. Martin
Department of Physics, University of Durham,
Durham DH1 3LE, England.

Contents

1. Introduction to deep inelastic scattering and partons
2. The QCD improved parton model
3. Determination of parton distributions
4. Summing LL(Q^2) via the Altarelli-Parisi equations
5. Summing double leading logs at small x and large Q^2: DLL($Q^2, 1/x$)
6. The LL($1/x$) sum and the BFKL equation
7. Shadowing and the GLR equation
8. Solutions and applications of the BFKL equation
9. Conclusions

FERMILAB
SEP 08 1993
LIBRARY

[1]Lectures given at the XXI International Meeting on Fundamental Physics, Miraflores de la Sierra, Madrid, 9-15 May 1993.

1. Introduction to Deep Inelastic Scattering and Partons

The precise determination of the partonic structure of the proton is important, since the parton densities are essential ingredients in the detailed analysis of any hard interaction involving a proton. Recent fixed-target deep-inelastic scattering data have considerably improved our knowledge of parton distributions, as we shall see in section 3 and, incidentally, provided an impressive confirmation of perturbative QCD. However it is the results that are just starting to come from the recently commissioned electron-proton collider, HERA, that are causing excitement. The reason is that HERA is probing the previously unexplored small x regime where novel perturbative QCD effects are anticipated. The aim of these lectures is to cover the above topics and if possible to convey some of the excitement.

There are many excellent reviews of perturbative QCD and deep inelastic scattering, some of which are listed in ref. [1]. The generic diagram for deep inelastic scattering is shown in Fig. 1. The lower or hadronic vertex is described by two invariant kinematic variables $Q^2 \equiv -q^2$ and the Bjorken variable $x = Q^2/2p \cdot q$. "Deep" and "inelastic" refer to $Q^2 \gg M^2$ and $W^2 \equiv (p+q)^2 \gg M^2$ respectively, which ensure that perturbative QCD is applicable and that we are above the region of nucleon resonance production. M is the mass of the nucleon.

If we concentrate on the photon exchange contribution to $ep \to eX$ then the spin-averaged matrix element squared has the form $e^4 L_{\mu\nu} W^{\mu\nu}/Q^2$ where L is the known lepton tensor and W is the hadronic tensor associated with $\gamma p \to X$ transition. The general expression for W is (see, for example, [2])

$$MW^{\mu\nu} = F_1(x,Q^2)\left(-g^{\mu\nu} + \frac{q^\mu q^\nu}{q^2}\right) + F_2(x,Q^2)P^\mu P^\nu \qquad (1)$$

where $P^\mu \equiv p^\nu - (p \cdot q/q^2)q^\mu$. It satisfies $q_\mu W^{\mu\nu} = 0$ as required by current conservation. The structure functions F_i are arbitrary functions of the kinematic variables x and Q^2 describing the $\gamma p \to X$ transition. The differential cross-section for $ep \to eX$ is readily shown to be

$$\frac{d^2\sigma}{dx dQ^2} = \frac{4\pi\alpha^2}{xQ^4}[y^2 x F_1(x,Q^2) + (1-y)F_2(x,Q^2)] \qquad (2)$$

where $y = 2p \cdot q/s$. Thus the F_i can be obtained from experiment with x, Q^2 and y determined from, for example, the energies and directions of the incident and outgoing electrons.

The basic idea of the original parton model was that at large Q^2 the photon-proton interaction can be expressed as the sum of incoherent scatterings from point-like quark constituents, which behave as if they were free inside the proton during the interaction, see Fig. 2. The argument is that the scattering occurs over a short timescale of order $1/\sqrt{Q^2}$ during which the photon sees a frozen state of non-interacting quarks

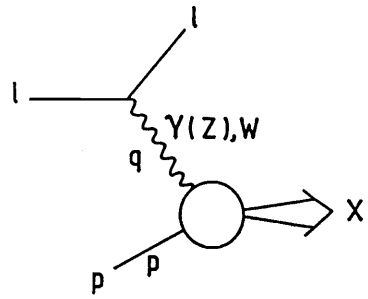

Figure 1: Deep inelastic lepton-proton scattering, $\ell p \to \ell X$. The processes $ep \to eX$ and $\nu p \to \mu X$, for example, proceed via γ(or Z) and W exchange respectively.

and that the final hadronization process occurs long after. If this is the case the differential cross section for $ep \to eX$ is of the form

$$\frac{d^2\sigma}{dx dQ^2} = \sum_i \int d\zeta f_i(\zeta) \frac{d^2\sigma_i}{dx dQ^2} \tag{3}$$

where $f_i(\zeta)$ is the probability of finding quark i in the proton with a fraction ζ of its momentum. The cross section for electron-quark elastic scattering is

$$\frac{d\sigma_i}{dQ^2} = \frac{4\pi\alpha^2}{\hat{t}^2} e_i^2 \tfrac{1}{2} \left(\frac{\hat{s}^2 + \hat{u}^2}{\hat{s}^2} \right) \tag{4}$$

in terms of the electron-quark subprocess variables. Using $\hat{t} = t = -Q^2$ and $\hat{u}/\hat{s} = u/s = (y-1)$ we have

$$\frac{d^2\sigma_i}{dx dQ^2} = \frac{4\pi\alpha^2}{Q^4} e_i^2 \tfrac{1}{2} [1 + (1-y)^2] \delta(x - \zeta), \tag{5}$$

where the δ-function arises from energy-momentum conservation and the neglect of the mass of the outgoing quark, that is $(\zeta p + q)^2 = 0$ which gives $\zeta = Q^2/2p \cdot q = x$. Inserting (5) into (3) and comparing with (2) gives

$$\begin{aligned} \frac{F_2}{x} = 2F_1 &= \sum_q \int d\zeta f_q(\zeta) e_q^2 \delta(x - \zeta) \\ &= \sum_q e_q^2 f_q(x). \end{aligned} \tag{6}$$

The equality $F_2 = 2xF_1$, which is only true in this naive quark model, is a direct consequence of the spin $\frac{1}{2}$ character of the quarks. Also we see that in the naive model the structure functions $F_i(x, Q^2)$ are predicted to scale; that is they are functions of a single variable, the so-called Bjorken scaling variable, $x = Q^2/2p \cdot q$.

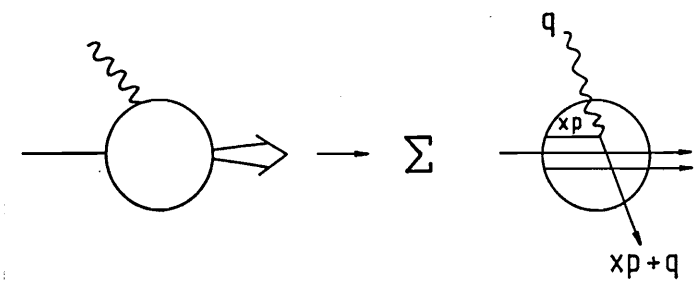

Figure 2: The quark parton model approximation of the hadronic vertex of Fig. 1. The sum is over all the quark (antiquark) constituents of the proton; p is the 4-momentum of the proton and the fraction ζ carried by the struck quark is equal to Bjorken x.

In addition to the three "valence" quarks (uud) which carry its quantum numbers, the proton also contains an infinite "sea" of $q\bar{q}$ pairs. When probed at a scale Q all sea quark flavours with $m_q \lesssim Q$ are active. Thus we may write

$$f_u(x) \equiv u(x) = u_v(x) + u_{sea}(x) \tag{7}$$

$$f_{\bar{u}}(x) \equiv \bar{u}(x) = u_{sea}(x) \tag{8}$$

with the constraint

$$\int_0^1 (u - \bar{u}) dx = \int_0^1 u_v dx = 2, \tag{9}$$

and analogous relations for $d, \bar{d}$ with, in this case, the sum rule constraint set equal to 1 valence quark.

From (6) we see that the quark parton model predicts

$$F_2^{ep} = x \left[\tfrac{4}{9} u + \tfrac{1}{9} d + \tfrac{1}{9} s + \tfrac{4}{9} \bar{u} + \ldots \right]. \tag{10}$$

For neutrino deep-inelastic scattering $\nu p \to \ell X$ the virtual W^+ probe measures the quark distributions weighted by the square of the weak charges

$$F_2^{\nu p} = 2x[d + s + \bar{u} + \bar{c}]. \tag{11}$$

Neutrino scattering involves a third structure function F_3, arising from the parity-violating $\epsilon_{\mu\nu\alpha\beta} p_\alpha q_\beta$ term in (1), which has the expansion

$$xF_3^{\nu p} = 2x[d + s - \bar{u} - \bar{c}] \tag{12}$$

with the antiquarks contributing with a minus sign. The expressions for the structure functions of the neutron are obtained from those of the proton by the interchanges $u \leftrightarrow d$ and $\bar{u} \leftrightarrow \bar{d}$. The antineutrino structure functions are obtained from the

neutrino functions by the interchange $q \leftrightarrow \bar{q}$, together with the insertion of an overall minus sign for xF_3.

Experimental measurements of the structure functions for deep inelastic $\mu p, \mu D \to \mu X$ and $\nu N \to \mu X$ scattering were used to estimate the $q(x)$ distributions and early on it was found

$$\sum_q \int_0^1 x(q(x) + \bar{q}(x))dx \simeq 0.5 \tag{13}$$

which indicated that the quarks only carry about half the momentum of the proton. The remainder was attributed to gluon constituents of the proton and indeed was some of the first (early) indirect evidence for the existence of the gluon.

2. The QCD improved parton model

With the advent of QCD it became clear that the quarks cannot be regarded as completely free when struck, but couple to gluons, and that the naive quark parton model is the zeroth order approximation in a perturbative expansion in α_s. In other words the proton is not simply composed of three point-like "valence" quarks but as Q^2 increases the photon (or W) resolves more and more substructure of the proton. For example, the photon may scatter one of a pair of "sea" quarks which originate from a gluon ($g \to q\bar{q}$) itself radiated from one of the valence quarks. Indeed the resolution increases with increasing Q^2 so that the apparent number of partons which share the proton's momentum increases, and hence there is an increased chance of finding a quark at small x and a decreased chance of finding one at high x. Such scale-violating Q^2 dependence is evident in the data, see, for example, Fig. 3.

In order to see whether the observed behaviour is in line with QCD expectations we must calculate the higher order (QCD) corrections to $\gamma^* q \to q$. The corrections up to $O(\alpha_s^2)$ are shown, and discussed in detail, in the lectures by van Neerven [3]. These important calculations are very involved and so here we give an introductory discussion concentrating on the lowest order, $O(\alpha_s)$, corrections. The relevant diagrams are shown in Fig. 4. The calculations involve loop and phase space integrals (since for an inclusive process we have to integrate over the outgoing parton momenta). Most of these integrals are divergent and have to be regulated. It is standard to use dimensional regularisation in which the calculations are performed in $n = 4 + \epsilon$, rather than 4, dimensions and where the singularities are identified as $(1/\epsilon)^p$ poles with $p = 1, 2$ etc. Most of the singularities are no problem. The ultraviolet singularities are removed by coupling constant renormalization, leading to a running coupling. Infrared singularities cancel between real and virtual contributions. Final state "mass or collinear" singularities (which arise when the momentum of two massless outgoing particles become parallel) cancel in an inclusive process. This leaves the initial state "mass or collinear" singularities. These must be removed if the parton model is to survive.

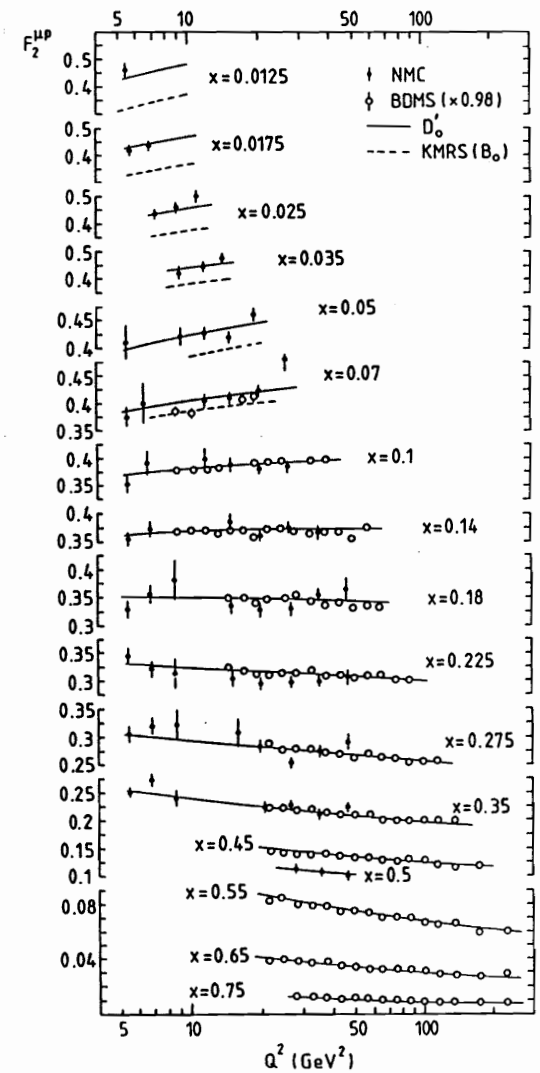

Figure 3: The BCDMS [4] and NMC [5] measurements of $F_2^{\mu p}$, together with the fits by KMRS [6] and MRS [9]. The NMC data were not available for KMRS. The figure is taken from ref. [9].

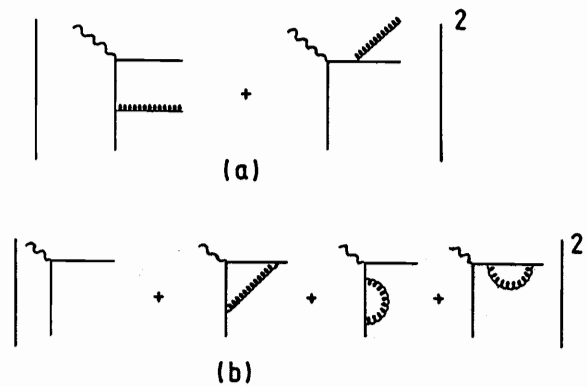

Figure 4: The $O(\alpha_s)$ corrections to $\gamma^* q \to q$.

If the $O(\alpha_s)$ corrections are included then the parton model formula[2] takes the modified form

$$\frac{F_2}{x} = \sum_q \int_x^1 \frac{dy}{y} f_q(y) e_q^2 \left[\delta\left(1-\frac{x}{y}\right) + \frac{\alpha_s}{2\pi}\left\{P\left(\frac{x}{y}\right)\log\frac{Q^2}{\mu^2} + R\left(\frac{x}{y}\right)\right\}\right] \tag{14}$$

where P and R are known calculable functions. The offending collinear divergence shows up in the $\log Q^2/\mu^2$ term which arises when the gluon in $\gamma^* q \to qg$ is emitted parallel to the incoming quark. It comes from t-channel quark exchange (the first diagram of Fig. 4) which gives a contribution

$$\frac{\alpha_s}{2\pi} P\left(\frac{x}{y}\right) \int_{\mu^2}^{\sim Q^2} \frac{dk_T^2}{k_T^2} \qquad \text{with} \qquad P(z) = \frac{4}{3}\left(\frac{1+z^2}{1-z}\right) \tag{15}$$

where k_T is the transverse momentum of the emitted gluon and $\hat{t} = -k_T^2/(1-z)$ with $z = x/y$. (At first sight we would have expected the t-channel quark propagator to lead to a factor $1/k_T^4$ in the amplitude squared, but helicity conservation at the gluon vertex weakens the collinear singularity by introducing a factor k_T^2 in the numerator.) Thus μ in (14) and (15) is a regulator introduced specifically to avoid the collinear singularity (which occurs when $k_T \to 0$).

These collinear or mass singularities appear to pose a real threat to the validity of the parton model. However they can be removed by factorizing them out of the partonic subprocess and absorbing them in the "bare" parton densities $f_q(y)$. This

[2]The fractional momentum variable ζ of (6) is from now on denoted by y, which is not to be confused with the deep inelastic variable y of (2) which we do not use again.

renormalization procedure is called "mass factorization". For the parton model to be useful the renormalized parton densities $f_q(y, Q^2)$ must be process independent and so the mass singularities must be universal. That is they must be the same for F_1 and F_2 and for Drell-Yan, jet production etc. Indeed this proves to be the case to all orders in perturbation theory. Since the $\log Q^2$ terms are absorbed into f_q the renormalized parton densities are Q^2 dependent, that is $f_q(y) \to f_q(y, Q^2)$, or to be more correct $f_q^{\text{bare}}(y) \to f_q^{\text{ren}}(y, Q^2)$.

After mass factorization (14) takes the form

$$\frac{F_2}{x} = \sum_q \int_x^1 \frac{dy}{y} f_q(y, M^2) e_q^2 \left[\delta\left(1-\frac{x}{y}\right) + \alpha_s C_2^q\left(\frac{x}{y}, \frac{Q^2}{M^2}\right)\right] \tag{16}$$

where the renormalized distributions are

$$f_q(x, M^2) = f_q(x) + \frac{\alpha_s}{2\pi}\int_x^1 \frac{dy}{y} f_q(y)\left\{P\left(\frac{x}{y}\right)\log\frac{M^2}{\mu^2} + R'\left(\frac{x}{y}\right)\right\}. \tag{17}$$

It is easy to check that the substitution of (17) into (16) reproduces (14) with C_2^q having a logarithmic dependence on Q^2/M^2. The separation of the singular part of the partonic subprocess (that is, of [...] in (14)) from the remaining finite part (the [...] in (16)) takes place at "mass factorization" scale M (often chosen to be equal to Q). The scale M separates the short distance ("partonic") effects from the long distance ("hadronic") effects. The finite part of the partonic process remaining in the [...] of (16) is thus infrared safe and independent of the long distance effects characterised by μ. It does not depend on which hadron is involved, but rather is specific to the partonic subprocess, $\gamma^* q \to q$ with QCD corrections. In contrast the renormalized parton distributions $f_q(x, M^2)$, which have absorbed all the infrared sensitivity, are specific to the hadron. However the crucial observation is that they are universal in the sense that the same distribution enters whenever the hadron enters a hard interaction. Moreover the renormalized distributions $f_q(x, M^2)$, unlike the bare distributions $f_q(x)$, are finite. This can be seen from (16) since the measurable F_2 is finite and [...] is finite by construction. It is clear from (17), with its arbitrary μ^2 behaviour, that there is no absolute prediction for $f_q(x, M^2)$. However QCD does give the M^2 dependence. From (17) we have

$$\frac{df_q(x, M^2)}{d\log M^2} = \frac{\alpha_s}{2\pi}\int_x^1 \frac{dy}{y} f_q(y, M^2) P\left(\frac{x}{y}\right). \tag{18}$$

The factorization scale M leading to the "running" of $f_q(x, M^2)$ therefore plays an analogous role to the renormalization scale m, that is needed to remove the ultraviolet divergences and which leads to the "running" of $\alpha_s(m^2)$. (For simplicity we have not shown, or discussed, the coupling constant renormalization but implicitly assumed that it has been done; usually m is also set equal to Q.) Eq. (18), known as the Altarelli-Parisi evolution equation, is the analogue of the β function equation specifying the behaviour of $\alpha_s(m^2)$ as a function of $\log m^2$.

Clearly the separation shown in (16) of the singular and non-singular parts of [...] in (14) is not unique. As long as the collinear singularity is absorbed into $f_q(x, M^2)$ we can add any additional finite parts we wish. We must therefore specify a "factorization scheme", and use it consistently from process to process. Two schemes occur frequently in the literature. By far the most common is the $\overline{\text{MS}}$ (or modified minimal subtraction) scheme in which only the $(1/\epsilon)^p$ pole terms (and the $\frac{1}{2}(\gamma_E - \log 4\pi)$ that naturally accompanies these poles) are absorbed. The other is the DIS scheme in which all the subprocess QCD corrections to the particular structure function F_2 are swept into $f_q(x, M^2 = Q^2)$, so that we have simply

$$\frac{F_2(x,Q^2)}{x} = \sum_q e_q^2 f_q(x,Q^2). \tag{19}$$

The disadvantage is that the corrections for the other structure functions, and for other processes, then become more complicated.

To determine the parton distributions we must turn to experiment. The procedure is to parametrize the x dependence of $f_i(x, Q_0^2)$ at some scale Q_0^2 and then to evolve in Q^2 using the Altarelli-Parisi equations, (18), to specify the $f_i(x, M^2 = Q^2)$ at all values of x and Q^2 where deep inelastic and related data exist. Using (16), and analogous expressions, we then perform a global fit to the data to find the optimum value of the parameters describing the initial distributions. Important ingredients are therefore the (coefficient) functions $C_2^q(x/y)$ of (16) and the (splitting) functions $P(x/y)$ of (18), both of which have calculable QCD perturbative expansions in α_s. Our outline discussion has only been to $O(\alpha_s)$. A much more detailed and informed discussion, including the $O(\alpha_s^2)$ contributions, is given in the lectures by van Neerven [3] in these proceedings. There he describes not only how all the leading $\alpha_s^n \log^n(Q^2/\mu^2)$ singular terms are absorbed, but also the inclusion of the next-to-leading logs, $\alpha_s^n \log^{n-1}(Q^2/\mu^2)$, as well. These are important calculations and the resulting QCD expansions for the coefficient and splitting functions up to and including $O(\alpha_s^2)$ are used in the global analyses described in section 3. Clearly the higher the order of α_s that can be included the less the dependence of the results on the arbitrary choice of scales.

At $O(\alpha_s)$ we note that we need to sum and absorb the whole series of $[\alpha_s(Q^2) \log(Q^2/\mu^2)]^n$, terms with $n = 1, 2...$, since, although $\alpha_s(Q^2)$ decreases like $1/\log Q^2$, the series does not converge as $Q^2 \to \infty$. We shall explain in section 4 how the iterative Altarelli-Parisi equations effectively "re-sum" this series of leading logs.

Even at $O(\alpha_s)$ our discussion is incomplete. We have only included the corrections to $\gamma^* q \to q$ coming for $\gamma^* q \to qg$. To $O(\alpha_s)$ we must also include contributions where a gluon in the initial state produces a quark-antiquark pair which the virtual photon then probes, that is the process $\gamma^* g \to q\bar{q}$. The evolution equation (18) then becomes

$$\frac{dq(x,Q^2)}{d\log Q^2} = \frac{\alpha_s(Q^2)}{2\pi} \int_x^1 \frac{dy}{y} \left[P_{qq}\left(\frac{x}{y}\right) q(y,Q^2) + P_{qg}\left(\frac{x}{y}\right) g(y,Q^2) \right] \tag{20}$$

where, to lowest order in α_s, we find (cf. (15))

$$P_{gg}(z) = \frac{4}{3}\frac{1+z^2}{1-z}, \qquad P_{qg}(z) = \frac{1}{2}[z^2 + (1-z)^2].$$

We have been cavalier about the running of α_s and it might cause concern to see that $\alpha_s(Q^2)$ suddenly appears in (20). We may trace the origin of this back to (15) which, for running $\alpha_s(m^2) = 2\pi/b\log(m^2/\Lambda^2)$, should read

$$P\left(\frac{x}{y}\right) \int^{\sim Q^2} \frac{dk_T^2}{k_T^2} \frac{\alpha_s(k_T^2)}{2\pi} = \frac{P}{b} \log\left(\log\frac{Q^2}{\Lambda^2}\right). \tag{21}$$

Following this through we have

$$\frac{dq}{d\log Q^2} = \frac{1}{b\log(Q^2/\Lambda^2)} \int ... = \frac{\alpha_s(Q^2)}{2\pi} \int ...$$

as in (20).

To complete the description, there is also an equivalent equation to (20) giving the evolution of the gluon distribution

$$\frac{dg(x,Q^2)}{d\log Q^2} = \frac{\alpha_s(Q^2)}{2\pi} \int_x^1 \frac{dy}{y} \left[P_{gg}\left(\frac{x}{y}\right) g(y,Q^2) + \sum_q P_{gq}\left(\frac{x}{y}\right) q(y,Q^2) \right] \tag{22}$$

with

$$P_{gg}(z) = 6\left(\frac{z}{1-z} + \frac{1-z}{z} + z(1-z)\right), \qquad P_{gq}(z) = \frac{4}{3}\frac{1+(1-z)^2}{z}. \tag{23}$$

Equations (20) and (22) suggest a classical interpretation of evolution where as Q^2 increases a parton i splits into partons j and k carrying fractions z and $(1-z)$ of its momentum respectively with probability $\alpha_s P_{ij}(z)/2\pi$, per unit of $\log(Q^2/Q_0^2)$. Of course this classical probabilistic interpretation is simply a verbal description of the leading order QCD evolution and such an intuitive picture cannot be maintained at higher orders.

We see that P_{qq} and P_{gg} have infrared singularities at $z = 1$ corresponding to the emission of soft gluons. These singularities are cancelled by virtual graphs (Fig. 4(b)), which are proportional to $\delta(1-z)$ since a virtual gluon cannot change the momentum of a parton. We can implement this cancellation by replacing the singular factor by a distribution

$$\frac{1}{1-z} \longrightarrow \frac{1}{(1-z)_+} \tag{24}$$

defined such that for a smooth function $f(z)$

$$\int_0^1 dz \frac{f(z)}{(1-z)_+} = \int_0^1 dz \frac{f(z) - f(1)}{(1-z)}. \tag{25}$$

In terms of this "plus prescription" we may write

$$P_{qq}(z) \;=\; \frac{4}{3}\frac{1+z^2}{(1-z)_+} + c_q\delta(1-z) \tag{26}$$

where the coefficient c_q can be found by explicitly evaluating the virtual contributions. More simply we can determine c_q by noting that the probability $P_{qq}(z)$ must satisfy the constraint

$$\int_0^1 P_{qq}(z)dz \;=\; 0 \tag{27}$$

which expresses the fact that the total number of quarks minus antiquarks is conserved. This requires $c_q = 2$. Similarly using overall momentum conservation we can show that the coefficient of the $\delta(1-z)$ term in $P_{gg}(z)$ is $c_g = 11/2 - n_f/3$.

3. Determination of parton distributions

As mentioned above, the parton distributions at some scale must be determined by experiment. The basic procedure is to parametrize the x dependence of $f_i(x, Q_0^2)$ at some low Q_0^2 but where Q_0^2 is sufficiently large for perturbative QCD to be applicable. Then we evolve up in Q^2 using the next-to-leading order Altarelli-Parisi equations to determine $f_i(x, Q^2)$ at all values of x and Q^2 where deep-inelastic and related data exist, and in this way we are able to perform a global fit to the data.

There is a long history of determining parton distributions from deep-inelastic data. Table 1 lists just the next-to-leading order analyses, together with the data fitted. The most significant recent (pre-HERA) experimental developments are the new NMC measurements [5] of $F_2^{\mu p}$ and $F_2^{\mu n}$ (or rather $F_2^{\mu D}$) and the CCFR measurements [11] of $F_2^{\nu N}$ and $xF_3^{\nu N}$. They have had a profound impact on our knowledge of parton distributions, especially for $x \lesssim 0.1$. Only the MRS('92) and CTEQ('93) analyses (that is the last three in Table 1) were able to incorporate these new data, and so should be able to provide a more reliable basis for extrapolation to smaller x. Figure 3 serves to highlight the problems associated with the extrapolation. It shows (dashed curves) an earlier KMRS global fit [6] which included the BCDMS data, together with the new MRS('92) fit to both BCDMS and the new NMC data sets. We see that extrapolations of the old solutions considerably undershoot the new data at small x. The new quark distributions are therefore much larger at small x. On the other hand for $x \gtrsim 0.1$ there is no change; we see both the "old" and "new" μp data and the partons are all in excellent agreement with each other.

As is apparent from Table 1, the parton distributions, f_i, are determined from global fits to a wide range of deep inelastic and related data. The deep-inelastic muon and neutrino data pin down the valence and sea quark distributions, but hardly constrain the gluon distribution, which only enters directly at next-to-leading order; essentially the only constraint is the momentum sum rule which shows that the gluon

carries just less than 50% of the proton's momentum at Q_0^2. On the other hand the gluon enters at leading order in prompt photon production. Indeed for "large" p_T photons produced by $pp \to \gamma X$, the dominant QCD subprocess is $gq \to \gamma q$, in contrast to $p\bar{p} \to \gamma X$ where the annihilation process $q\bar{q} \to \gamma g$ is much more important. The relevant data are from the WA70 collaboration [12] which determine the gluon in the region $x \sim 0.35$. Combined with the momentum sum rule constraint, this gives an input gluon behaviour $(1-x)^{5.3}$ at large x. Data for the Drell-Yan $pN \to \mu^+\mu^- X$ process, which is mediated at leading order by $q_v\bar{q}_{sea} \to \gamma^*$, constrain the $(1-x)^{\eta_s}$ behaviour of the sea quark distributions. Finally data on W production at $\bar{p}p$ colliders impose tight constraints on the u and d distributions, particularly when the accurate NMC measurements of $F_2^{\mu p}/F_2^{\mu p}$ have to be fitted simultaneously.

To be specific we discuss the MRS('92) analysis. The input parametrizations at $Q^2 = Q_0^2$ (= 4 GeV^2) of the gluon (g), valence (u_v, d_v) and sea ($\bar{u} = \bar{d} \simeq 2\bar{s}$) quark distributions each are assumed to have the form

$$xf_i(x, Q_0^2) \;=\; A_i\, x^{-\lambda_i}(1-x)^{\beta_i}(1 + \gamma_i x^{\frac{1}{2}} + \delta_i x) \tag{28}$$

where $u \equiv f_u = u_v + u_{sea}$, $\bar{u} = u_{sea}$ etc. and where the parameters $A_i, \lambda_i, \beta_i, \gamma_i, \delta_i$ are to be determined by the fit to the data. Not all the parameters A_i are free since we require

$$\sum_i \int xf_i(x) \;=\; 1 \tag{29}$$

by momentum conservation, and

$$\int (u - \bar{u})dx \;=\; 2, \qquad \int (d - \bar{d})dx \;=\; 1 \tag{30}$$

due to the flavour content of the proton. Moreover we have some idea of the values of the parameters λ_i and β_i from the expected behaviour of the parton distributions as $x \to 0$ and $x \to 1$ respectively. Naive counting rule estimates suggest

$$f_i \;\sim\; (1-x)^{2n_s - 1} \tag{31}$$

as $x \to 1$, where n_s is the minimum number of spectator partons accompanying the probed parton. So for valence quarks, gluons and sea quarks we expect $\beta_i \simeq 2n_s - 1$ to be 3, 5 and 7 respectively. Naive Regge arguments suggest $\lambda_{i=v} \approx \alpha_M(0) - 1 \approx -\frac{1}{2}$ since in this model the $x \to 0$ (i.e. $p \cdot q \to \infty$) behaviour of valence quark distributions are controlled by the intercept $\alpha_M(0)$ of the $\rho - a_2 - \omega - f_2$ meson Regge trajectory. On the other hand $\lambda_{sea} \approx \lambda_g \simeq \alpha_P(0) - 1 \approx 0$ if we assume the Pomeron has intercept about 1.

Of course the above arguments only give estimates of the parameters λ_i and β_i. In fact, as we shall see, there are theoretical reasons from perturbative QCD to believe that $\lambda_{sea} \approx \lambda_g \approx 0.5$. We thus must distinguish a "soft" pomeron (applicable in the Regge domain, $Q^2 \approx 0$) which would suggest a small x behaviour $xg, x\bar{q} \sim x^{-\lambda}$ with

	μ-DIS	ν-DIS	Prompt γ	D-Yan	W,Z
MRS '88	EMC + ..	CDHSW	AFS(+J/ψ)	-	-
DFLM '88	(EMC + ..)	CHARM + ..	-	E288 + ..	-
ABFOW '89	BCDMS	-	WA70	-	-
HMRS '90	EMC BCDMS NMC(n/p)	CDHSW	WA70	E605	-
MT '90	EMC BCDMS	CDHSW	-	E288 E605	-
KMRS '90 (sets B_0,B_-)	BCDMS NMC(n/p)	CDHSW	WA70	E605	-
MRS (Apr '92) (sets D_0,D_-)	BCDMS NMC(p,n)†	CDHSW CCFR†	WA70 ′	E605	(UA2, CDF)
MRS (Nov '92) (sets D'_0,D'_-)	BCDMS NMC(p,n)	CCFR	WA70	E605	(UA2, CDF)
CTEQ ('93)	BCDMS NMC(p,n)	CCFR	WA70 E706,UA6	E605	

Table 1: NLO determinations of parton distributions [8, 6, 7, 9, 10] together with the data used in the various analyses. Data marked † were used in preliminary form.

$\lambda \simeq \alpha_P(0) - 1 \approx 0$, or to be more precise 0.08, from a "hard" or "QCD" or "Lipatov" pomeron (applicable at Q^2 values where perturbative QCD is valid) which implies

$$xg, x\bar{q} \sim x^{-\frac{1}{2}} \tag{32}$$

for small x (see section 6). To illustrate the difference we will obtain parton sets with $\lambda_g = \lambda_{sea} = 0$ (sets D_0 and S_0) and a set with $\lambda_g = \lambda_{sea} = 0.5$ (set D_-).

Let us return to the input assumption that the sea quark distributions[3] satisfy $\bar{u} = \bar{d} = 2\bar{s}$. First the evidence that the strange sea is about half as weak as the non-strange seas comes from observations [14] of deep-inelastic dimuon production, $\nu N \to \mu^+\mu^- X$, for which the dominant subprocess is $\nu s \to \mu^-(c \to \mu^+)$. Secondly, although until recently all analyses assumed $\bar{u} = \bar{d}$, the new NMC data [5] indicate that this equality may not be exact. This is best seen in terms of the Gottfried sum rule

$$\begin{aligned} I_{\rm GSR} &\equiv \int_0^1 \frac{dx}{x}(F_2^{\mu p} - F_2^{\mu n}) \\ &= \int_0^1 [\tfrac{4}{9}(u+\bar{u}) + \tfrac{1}{9}(d+\bar{d}) - \tfrac{4}{9}(d+\bar{d}) - \tfrac{1}{9}(u+\bar{u})]dx \\ &= \tfrac{1}{3}\int_0^1 dx(u_v - d_v) + \tfrac{2}{3}\int_0^1 dx(\bar{u} - \bar{d}) \\ &= \tfrac{1}{3} \qquad \text{if } \bar{u} = \bar{d}. \end{aligned} \tag{33}$$

On the other hand NMC find [15]

$$\int_{0.004}^{0.8} \frac{dx}{x}(F_2^{\mu p} - F_2^{\mu n}) = 0.227 \pm 0.007(\text{stat.}) \pm 0.014(\text{sys.}) \tag{34}$$

at $Q^2 = 4$ GeV^2. A straightforward comparison of (10) and (11) implies $\bar{u} \neq \bar{d}$. To allow for this MRS [7] parametrize

$$\bar{d} - \bar{u} = Ax^{-\alpha}(1-x)^{\beta_s} \tag{35}$$

where $\alpha \approx \alpha_M(0)$ since the difference may be associated with the lack of Regge $\rho - a_2$ exchange degeneracy. When this is done (sets D_0,D_-) it is found $\bar{d} > \bar{u}$ and that $I_{\rm GSR}$ of (10) is about 0.26. It is interesting to note that it is still possible to maintain $\bar{u} = \bar{d}$ and obtain an equally good global description of deep-inelastic and related data but at the expense of a somewhat contrived small x behaviour of the valence distributions, see set S_0 of [7]. However it is more physical to allow $\bar{u} \neq \bar{d}$ and so the discussion will concentrate on sets D_0 and D_-. Fig. 5 summarizes this Gottfried sum rule discussion.

In addition to the parameters describing the input distributions there is the final important parameter, Λ_{QCD}, which specifies the running of α_s and which determines

[3] CTEQ [10] use freely parametrized input distributions for $\bar{u}$, $\bar{d}$ and $\bar{s}$. A critique of this approach is given in Ref. [13].

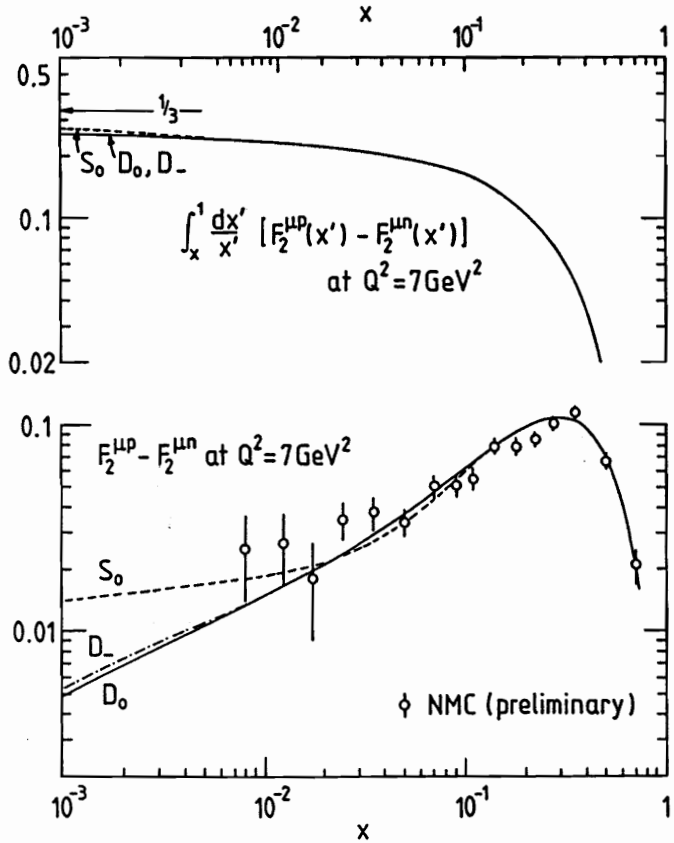

Figure 5: The upper curves give the accumulated contribution, $\int_x^1$, to the Gottfried sum rule, (33), as a function of x, the lower limit of integration. Predictions are shown for sets S_0, D_0 and D_- of partons of ref. [7]. The lower curves compare the integrand, $F_2^{\mu p} - F_2^{\mu n}$, with NMC data [16]. The figure is taken from ref. [7], see also [17].

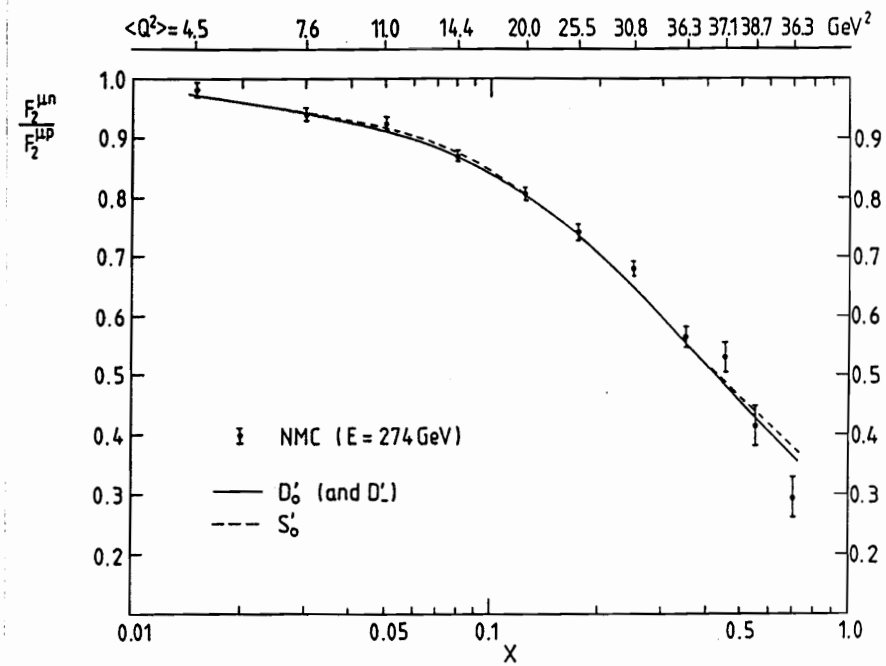

Figure 6: The description of the NMC data [5] for the structure function ratio $F_2^{\mu n}/F_2^{\mu p}$ given by the S_0', D_0' and D_-' sets of partons of ref. [9]. The mean Q^2 of the data varies with x as shown by the uppermost scale. The curves take this Q^2 dependence into account. The values of $F_2^{\mu n}$ have been obtained from μD data corrected for deuteron screening effects. The figure is taken from ref. [9].

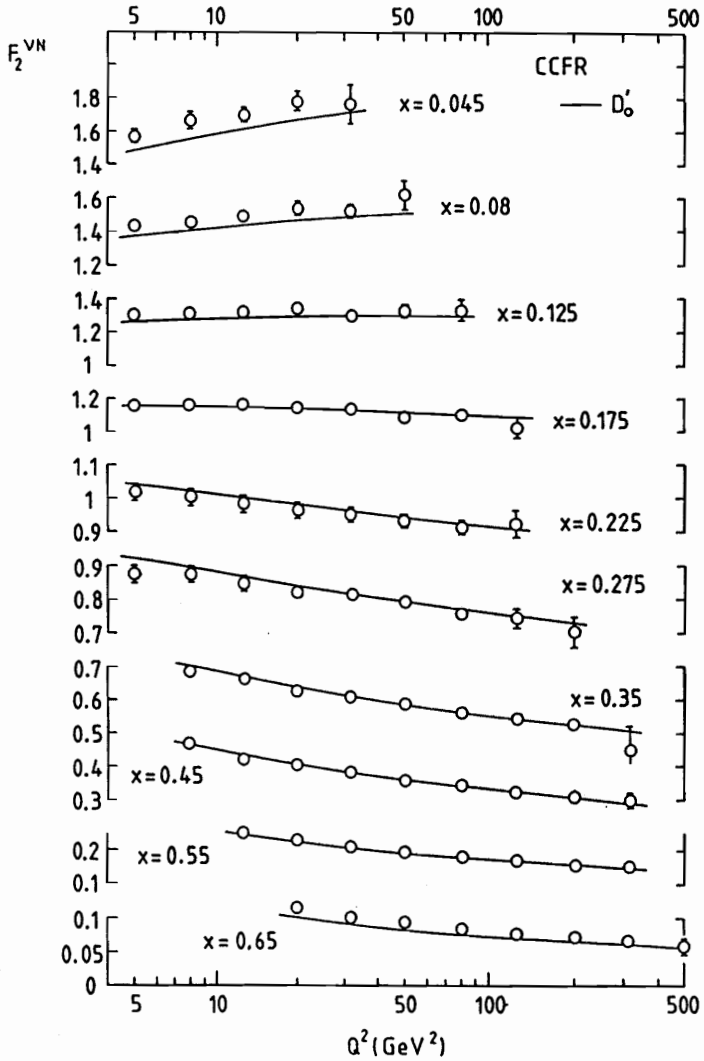

Figure 7: The continuous curves show the description of the CCFR [11] measurements of the $F_2^{\nu N}(x, Q^2)$ structure function by the D_0' set of partons [9]. The data are shown after correction for the heavy target effects and after the overall renormalization of 0.95 required by the global fit. The figure is taken from ref. [9].

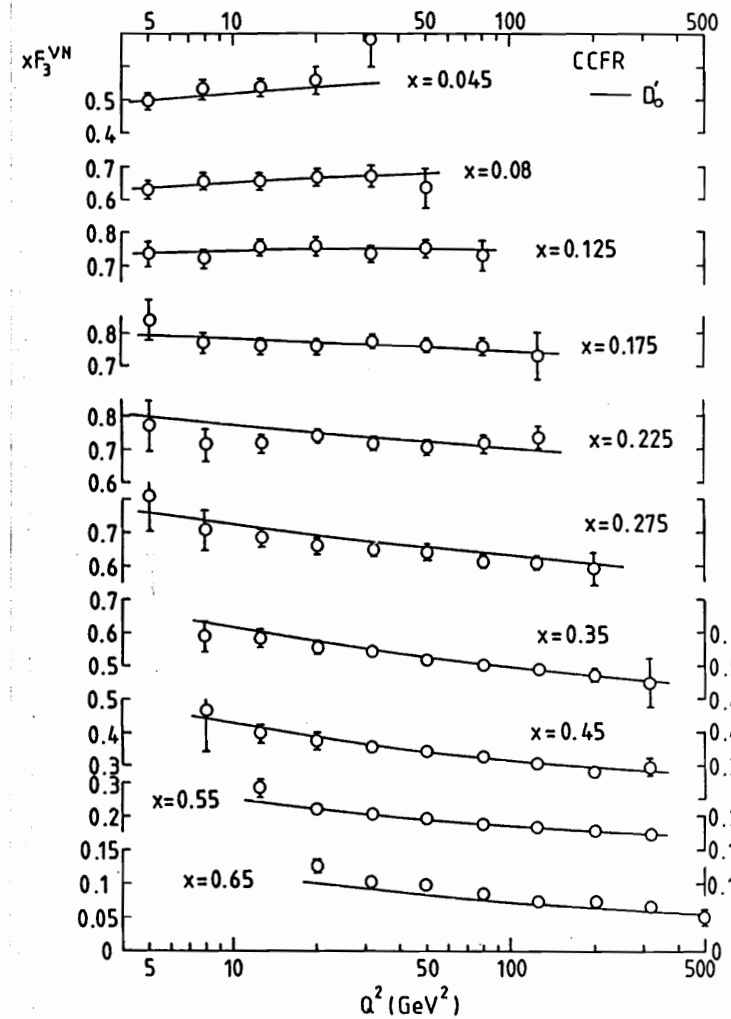

Figure 8: As for Fig. 7 but for the structure function $xF_3^{\nu N}(x, Q^2)$.

the rate of evolution in Q^2. We use the $\overline{\mathrm{MS}}$ scheme. Thus, in summary, MRS fit to deep inelastic and related data with a total of about 15 parameters. The quality of the fit to the recent high precision deep-inelastic data is shown in Figs. 3,6,7 and 8. Only data with $Q^2 > 5$ GeV^2 are fitted. The value of Λ is found to be [9]

$$\Lambda_{\overline{\mathrm{MS}}}(n_f = 4) \;=\; 230 \pm 55\mathrm{MeV} \tag{36}$$

which corresponds to

$$\alpha_s(M_z^2) \;=\; 0.112_5{}^{+0.004}_{-0.005}, \tag{37}$$

to be compared with $\alpha_s = 0.120 \pm 0.006$ which is the average of the LEP determinations.

We note that to determine $f_i(x, Q^2)$ from the evolution equations, (20) and (22), we only integrate over y from x up to 1. Thus the fits to the data do not involve, or determine, $f_i(x, Q^2)$ for values of x below that for which data exist. However the precision of the data means that we should now have reliable sets of parton distributions at least in the region $x \gtrsim 0.05$. Extrapolations outside the region of the data are notoriously unreliable. All we can do is to use the input parametric forms, together with the evolution equations, to extrapolate the various sets to small x to show the general trends.

Fig. 9 shows parton sets D_0' and D_-' where the latter set incorporate the singular "Lipatov-like" forms xg, $x\bar{q} \sim x^{-\frac{1}{2}}$ at small x. These two sets are essentially identical for $x \gtrsim 0.02$ (though there is some difference in the gluon that is necessary to conserve momentum), but they are dramatically different at small x. In particular Fig. 10 shows that they lead to very different predictions for F_2^{ep} in the HERA regime.

4. Summing LL(Q^2) via the Altarelli-Parisi equations

In preparation for the study of the small x region[4] it is useful to return to the Altarelli-Parisi equations and to show how they effectively resum the leading log Q^2 (LL(Q^2)) terms (see also ref. [21]). For simplicity consider a non-singlet quark distribution (e.g. $u - \bar{u}$), since it decouples from the evolution of the gluon distribution so that the (leading order) Altarelli-Parisi equation is simply

$$\begin{aligned} \frac{dq(x,Q^2)}{d\log Q^2} &= \frac{\alpha_s(Q^2)}{2\pi}\int_x^1 \frac{dy}{y} P_{qq}\left(\frac{x}{y}\right) q(y,Q^2) \\ &= \frac{\alpha_s(Q^2)}{2\pi}\int_0^1 dy \int_0^1 dz\,\delta(x - yz) P_{qq}(z) q(y,Q^2), \end{aligned} \tag{38}$$

which can be pictured as a "quark" of momentum fraction y splitting up into a "quark" of momentum fraction $x = zy$ and a gluon of momentum fraction

[4] Recent reviews of small x physics include those listed in ref. [19].

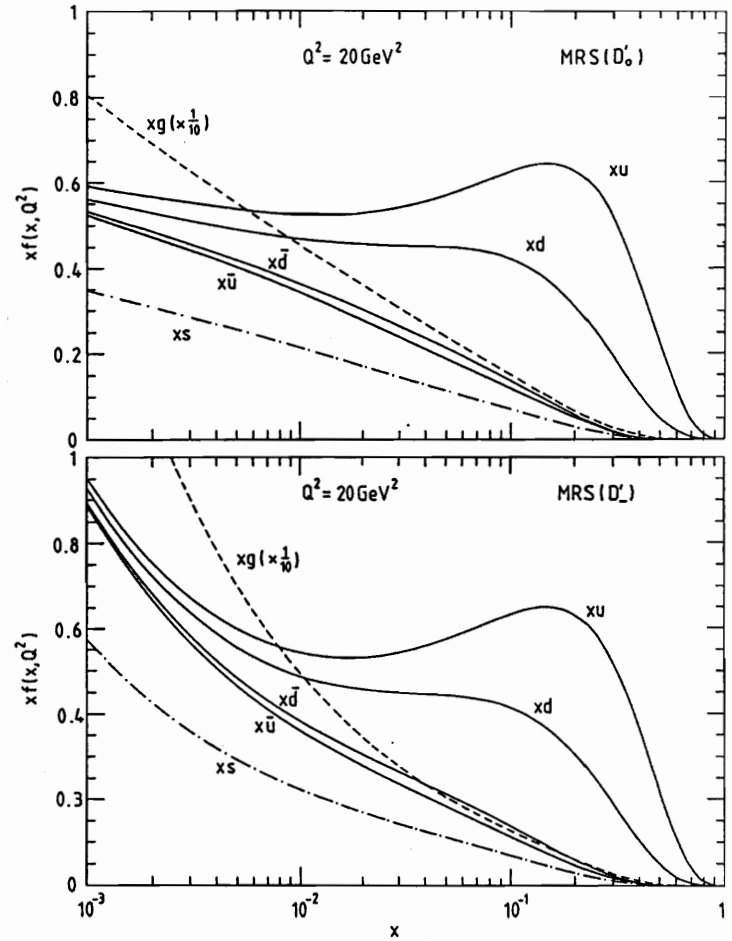

Figure 9: The parton distributions of the proton at $Q^2 = 20$ GeV^2 corresponding to (a) set D_0' and (b) set D_-' of the analysis of ref. [9]. Although the two sets are essentially identical in the x region of the data fitted ($x \gtrsim 0.05$) they differ greatly at small x due to the more singular input forms (32) used for the gluon and sea quarks in set D_-.

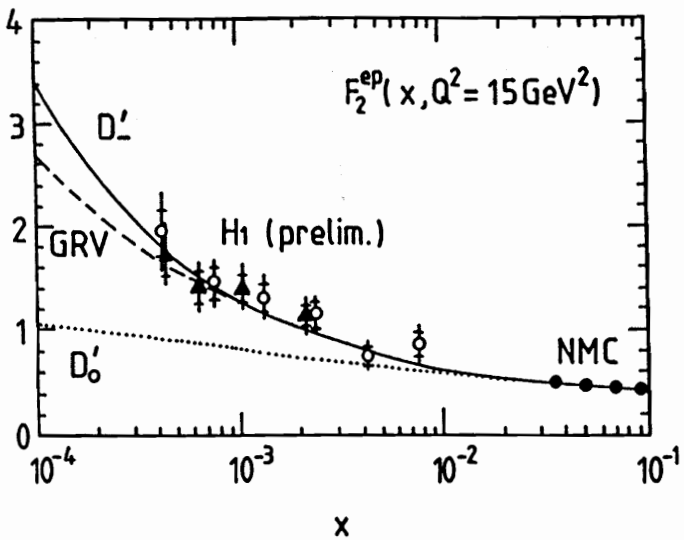

Figure 10: The predictions of F_2^{ep} obtained from extrapolations of D'_0, D'_- [9] and GRV [20] to small x. The new HERA data for F_2^{ep} [18] and the fixed target NMC measurements of $F_2^{\mu p}$ [5] are also shown. Only the latter data were fitted in [9].

$(1-z)y$; note that $y > x$. The Altarelli-Parisi equations can be solved either by direct numerical integration step-by-step in $\log Q^2$ or by inverting the moments of the x distribution. The first method is usually used in global analyses of the data of the type that were described in section 3. However here it is useful to introduce the moment analysis.

If we take the moments of (38) then the Altarelli-Parisi equation factorizes and the resulting differential equation can be solved to give their Q^2 evolution. From (38) we have

$$\int_0^1 \frac{dx}{x} x^n \frac{dq(x,Q^2)}{d\log Q^2} = \frac{\alpha_s(Q^2)}{2\pi} \int_0^1 dy \int_0^1 dz \int_0^1 \frac{dx}{x} x^n \delta(x - yz) P_{qq}(z) q(y, Q^2)$$
$$= \frac{\alpha_s(Q^2)}{2\pi} \int_0^1 \frac{dz}{z} z^n P_{qq}(z) \int_0^1 \frac{dy}{y} y^n q(y, Q^2),$$

which gives

$$\frac{dM_n(Q^2)}{d\log Q^2} = \frac{1}{b\log(Q^2/\Lambda^2)} A_n M_n(Q^2) \tag{39}$$

where

$$M_n(Q^2) \equiv \int_0^1 \frac{dx}{x} x^n q(x, Q^2), \tag{40}$$

$$A_n \equiv \int_0^1 \frac{dx}{x} x^n P_{qq}(x), \tag{41}$$

$$\alpha_s(Q^2) = \frac{1}{b\log(Q^2/\Lambda^2)}. \tag{42}$$

Eq. (39) can be readily solved giving

$$M_n(Q^2) = c_n \left(\log \frac{Q^2}{\Lambda^2}\right)^{A_n/b} \tag{43}$$

where c_n cannot be calculated from perturbation theory and so its value, via $M_n(Q_0^2)$, must be determined by experiment. In other words we only know the evolution

$$M_n(Q^2) = M_n(Q_0^2) \left[\frac{\alpha(Q_0^2)}{\alpha(Q^2)}\right]^{A_n/b} \tag{44}$$

and not the absolute values of the moments. It is straightforward to evaluate (41) and to show that $A_1 = 0$ and $A_n < 0$ for $n \geq 2$. The first result follows from (27) and the second simply reflects the expectation that as Q^2 increases the distribution $q(x, Q^2)$ decreases at large x and increases at small x.

Incidentally we note that we can recover the parton x distributions from the moments by taking an inverse Mellin transform. We analytically continue the moments into the complex n plane and use the inverse relation to (40)

$$q(x, Q^2) = \frac{1}{2\pi i} \int_{c-i\infty}^{c+i\infty} M(n, Q^2) x^{-n} dn \tag{45}$$

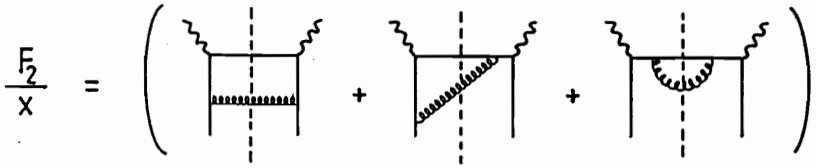

Figure 11: $O(\alpha_s)$ real gluon emission contributions to $F_2(x, Q^2)$.

where c is chosen such that the contour lies to the right of the singularities of M in n. However here the result we wish to use is (43).

To gain insight into how the Altarelli-Parisi equation sums the leading log Q^2 terms we return to Fig. 4(a). The resulting contribution to F_2 is shown in Fig. 11. While the sum of these graphs is gauge invariant, their relative importance depends on the choice of gauge. Dokshitzer [22] showed that in an axial gauge the log Q^2 term comes from the first graph, and that the LL(Q^2) sum comes from the sum of ladder graphs. An axial gauge is one in which the gluon has only the two physical polarization states. (In such a gauge we do not need unphysical ghost contributions which in general would be required to cancel the scalar polarization component of the gluon).

Here we shall use (43) to give a heuristic discussion of how the Altarelli-Parisi equation is equivalent to the LL(Q^2) sum of ladder diagrams. We write (43) as

$$\begin{aligned} M_n(Q^2) &= c_n \exp\left(\frac{A_n}{b}\log\left(\log\frac{Q^2}{\Lambda^2}\right)\right)^r \\ &= c_n \sum_r \frac{1}{r!}\left(\frac{A_n}{b}\log\left(\log\frac{Q^2}{\Lambda^2}\right)\right)^r \end{aligned} \tag{46}$$

and show that the rth term is equivalent to the ladder diagram with r rungs.

We begin with the 1-rung ladder of Fig. 12(a). This contribution was given in (14) which, with the help of (21), may be expressed as

$$\frac{F_2(x,Q^2)}{x} = \sum_q \int_x^1 \frac{dy}{y} q(y) e_q^2 P_{qq}\left(\frac{x}{y}\right) \int^{Q^2} \frac{dk_T^2}{k_T^2} \frac{\alpha_s(k_T^2)}{2\pi}. \tag{47}$$

Working to leading order, we rewrite the various factors in the form

$$\sum_q e_q^2 q(x,Q^2) = \sum_q e_q^2 \int_0^1 dz \int_0^1 dy q(y)\delta(x-yz) P_{qq}(z) \frac{1}{b}\log\left(\log\frac{Q^2}{\Lambda^2}\right) \tag{48}$$

which on taking moments gives

$$\int_0^1 \frac{dx}{x} x^n q(x,Q^2) = \int_0^1 \frac{dy}{y} y^n q(y) \int_0^1 \frac{dz}{z} z^n P_{qq}(z) \frac{1}{b}\log\left(\log\frac{Q^2}{\Lambda^2}\right), \tag{49}$$

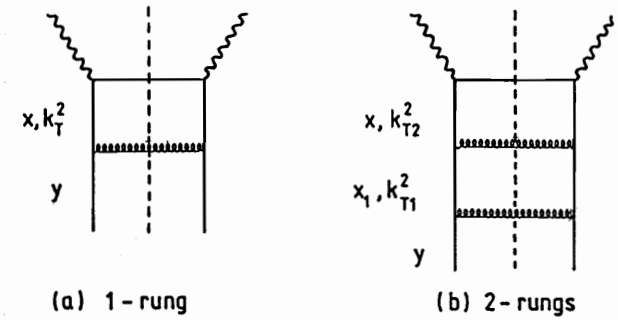

Figure 12: $O(\alpha_s)$ and $O(\alpha_s^2)$ "ladder" diagram contributions to $F_2(x, Q^2)$.

and so

$$M_n(Q^2)_{1-\text{rung}} = c_n \frac{A_n}{b}\log\left(\log\frac{Q^2}{\Lambda^2}\right), \tag{50}$$

where A_n is defined in (42) and

$$c_n \equiv \int_0^1 \frac{dy}{y} y^n q(y). \tag{51}$$

We have therefore identified the 1-rung contribution, (50), with the $r = 1$ term of (46).

We evaluate the 2-rung contribution in the same way, but now we have to integrate over the variables shown in Fig. 12(b). The LL(Q^2) contribution comes from the region of phase space that is "strongly ordered" in k_T^2

$$Q^2 \gg k_{T2}^2 \gg k_{T1}^2 \tag{52}$$

so that we effectively have the nested integrations

$$\begin{aligned} &\int^{Q^2} \frac{dk_{T2}^2}{k_{T2}^2} \frac{\alpha_s(k_{T2}^2)}{2\pi} \int^{k_{T2}^2} \frac{dk_{T1}^2}{k_{T1}^2} \frac{\alpha_s(k_{T1}^2)}{2\pi} \\ &= \frac{1}{2\pi b}\int^{Q^2} d\log\left(\log\frac{k_{T2}^2}{\Lambda^2}\right) \frac{1}{2\pi b}\log\left(\log\frac{k_{T2}^2}{\Lambda^2}\right) \\ &= \frac{1}{2\pi b}\frac{1}{2}\left[\log\left(\log\frac{Q^2}{\Lambda^2}\right)\right]^2. \end{aligned} \tag{53}$$

The integration over the longitudinal momenta, which we denote L(x), must satisfy the physical constraint

$$1 > y > x_1 > x, \tag{54}$$

which reflects the degradation of the proton momentum along the ladder. Thus we have

$$\begin{aligned} L(x) &\equiv \int_x^1 \frac{dx_1}{x_1} P_{qq}\left(\frac{x}{x_1}\right)\left[\int_{x_1}^1 \frac{dy}{y} P_{qq}\left(\frac{x_1}{y}\right) q(y)\right] \\ &= \int_0^1 dz \int_0^1 dx_1 \delta(x - x_1 z) P_{qq}(z)\left[\int_{x_1}^1 \frac{dy}{y} P_{qq}\left(\frac{x_1}{y}\right) q(y)\right]. \end{aligned} \tag{55}$$

We take moments so that the z and x_1 integrations factorize

$$\begin{aligned} \int \frac{dx}{x} x^n L(x) &= \int_0^1 \frac{dz}{z} z^n P_{qq}(z)\left\{\int_0^1 \frac{dx_1}{x_1} x_1^n \left[\int_{x_1}^1 \frac{dy}{y} P_{qq}\left(\frac{x_1}{y}\right) q(y)\right]\right\} \\ &= A_n \{c_n A_n\} = c_n A_n^2 \end{aligned} \tag{56}$$

where $\{...\}$ has precisely the form of the moments which occur in the 1-rung case and so can be factorized to give $c_n A_n$ exactly as in (47) to (50). Combining the results of the integrations over the transverse and longitudinal momenta, (53) and (56), we have

$$M_n(Q^2)_{2-\text{rung}} = c_n \frac{1}{2!}\left[\frac{A_n}{2\pi b}\log\left(\log\frac{Q^2}{\Lambda^2}\right)\right]^2 \tag{57}$$

which is precisely the $r = 2$ term of (46). It is straightforward to extend the argument and to verify that the LL(Q^2) resummation implicitly embodied in the Altarelli-Parisi equation, (38), is equivalent to summing ladder diagrams (in an axial gauge), with each additional rung giving an extra $\log(Q^2)$, or rather $\log(\log Q^2)$.

5. Summing double leading logs at small x and large Q^2: DLL($Q^2, 1/x$)

In the small x regime we encounter new logarithmic effects associated with $\log(1/x)$ contributions. These will need to be resummed. For simplicity we take α_s fixed. First we consider the case when

$$\alpha_s \log\frac{1}{x}\log\frac{Q^2}{Q_0^2} \sim 1 \tag{58}$$

but where $\alpha_s\log(1/x)$ and $\alpha_s\log(Q^2/Q_0^2)$ are both small. At small x the gluon dominates and so we keep only $g(x, Q^2)$. The Altarelli-Parisi equation which sums the double leading logs (i.e. the $[\alpha_s\log(1/x)\log(Q^2/Q_0^2)]^n$ terms) is

$$\frac{dg(x, Q^2)}{d\log Q^2} = \frac{\alpha_s}{2\pi}\int_x^1 \frac{dy}{y} P_{gg}\left(\frac{x}{y}\right) g(y, Q^2). \tag{59}$$

We speak of the double leading log (DLL) approximation based on the small x behaviour $P_{gg}(x) \approx 6/x$ (see (24)). Then (59) becomes

$$\frac{d(xg(x, Q^2))}{d\log Q^2} = \frac{3\alpha_s}{\pi}\int_x^1 \frac{dy}{y} y g(y, Q^2) \tag{60}$$

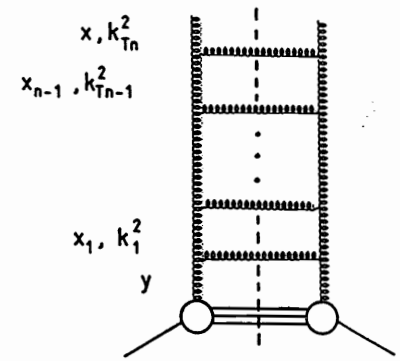

Figure 13: The n-rung gluon ladder diagram.

which can be solved directly to give the asymptotic behaviour

$$xg(x, Q^2) \sim \exp\left(2\left[\frac{3\alpha_s}{\pi}\log\frac{1}{x}\log\frac{Q^2}{Q_0^2}\right]^{\frac{1}{2}}\right). \tag{61}$$

Thus as $x \to 0$ we see that the DLL summation implies xg grows faster than any power of $\log(1/x)$.

Here it is useful to identify the DLL behaviour (61) with the sum of ladder diagrams. The n-rung diagram is shown in Fig. 13. Each additional rung, say rung i, brings in a factor (cf. (14) and (15))

$$\int \frac{dx_{i-1}}{x_{i-1}}\int dk_{Ti}^2\left\{\frac{\alpha_s}{2\pi}\frac{1}{k_{Ti}^2}P_{gg}\left(\frac{x_i}{x_{i-1}}\right)\right\} \approx \frac{3\alpha_s}{\pi}\int\frac{dx_{i-1}}{x_{i-1}}\int\frac{dk_{Ti}^2}{k_{Ti}^2}\left(\frac{x_{i-1}}{x_i}\right) \tag{62}$$

where the factor (x_{i-1}/x_i) will be absorbed to translate the result for $g(x, Q^2)$ into one for $xg(x, Q^2)$. As before we treat the integrations over the transverse and longitudinal momenta separately. Again the LL(Q^2) terms come from the strongly-ordered region

$$Q^2 \gg k_{Tn}^2 \gg ... \gg k_{T1}^2 \tag{63}$$

so that we have nested integrations

$$\left(\frac{3\alpha_s}{\pi}\right)^n \int^{Q^2}\frac{dk_{Tn}^2}{k_{Tn}^2}\int^{k_{Tn}^2}\frac{dk_{Tn-1}^2}{k_{Tn-1}^2}...\int^{k_{T2}^2}\frac{dk_{T1}^2}{k_{T1}^2} = \frac{1}{n!}\left(\frac{3\alpha_s}{\pi}\log\frac{Q^2}{Q_0^2}\right)^n. \tag{64}$$

In a similar way the LL($1/x$) terms arise from the strongly-ordered region

$$x \ll x_{n-1} \ll ...x_1 \ll y \tag{65}$$

so we also have the nested integrations

$$\int_x^1 \frac{dx_{n-1}}{x_{n-1}} \cdots \int_{x_2}^1 \frac{dx_1}{x_1} \int_{x_1}^1 \frac{dy}{y} y g(y, Q_0^2) \;=\; \frac{1}{n!}\left(\log\frac{1}{x}\right)^n G_0 \tag{66}$$

where G_0 is the small x limit of $xg(x, Q_0^2)$.

The DLL approximation for $xg(x, Q^2)$ is the sum of ladder diagrams, each of which is given by a product of forms of the type of (64) and (66),

$$xg(x, Q^2) \;=\; G_0 \sum_n \left(\frac{1}{n!}\right)^2 \left(\frac{3\alpha_s}{\pi} \log\frac{1}{x} \log Q^2\right). \tag{67}$$

The sum may be evaluated using the identity

$$\sum_n \left(\frac{1}{n!}\right)^2 \left(\frac{z^2}{4}\right)^n \;=\; I_0(z) \;=\; \frac{e^z}{\sqrt{2\pi z}} \text{ as } z \to \infty, \tag{68}$$

where I_0 is a modified Bessel function, which gives

$$xg(x, Q^2) \;\sim\; G_0 \exp\left(2\left[\frac{3\alpha_s}{\pi} \log\frac{1}{x} \log Q^2\right]^{\frac{1}{2}}\right) \tag{69}$$

in the DLL limit.

6. The LL($1/x$) sum and the BFKL equation

Fig. 14 summarises our discussion so far. The figure shows the strongly-ordered momentum configurations that gave rise to the LL(Q^2) and DLL($Q^2, 1/x$) approximations, which were discussed in sections 4 and 5 respectively. Recall that the DLL approximation only includes the LL($1/x$) terms that are accompanied by LL(Q^2). For HERA we need QCD predictions for small x but moderate Q^2. Starting from a knowledge of $g(x_0, Q^2)$ (with say $x_0 \gtrsim 0.01$) we wish to predict $g(x, Q^2)$ at smaller x, that is to evolve in the upwards direction in Fig. 14 at moderate Q^2. For moderate Q^2 we must sum the LL($1/x$) terms but keep the full Q^2 dependence, not just the LL(Q^2) terms. Clearly we must relax the strong ordering of the k_T's which gave the LL(Q^2) behaviour and integrate over the full k_T phase space.

As in the other cases, we can picture the LL($1/x$) behaviour as a sum of "ladder" diagrams, but now the QCD calculation is much more involved. The resulting structure does indeed look like a summation of ladder diagrams but actually they are only an effective representation for a whole set of Feynman diagrams, most of which are of non-ladder form, which were originally[5] summed by Fadin, Kuraev, Lipatov and

[5] More recently an alternative approach, based on the introduction of a non-Sudakov form factor, has been proposed by Marchesini et al. [24]. In this way they have managed to derive an equation which reduces to the BFKL equation at small x and to the Altarelli-Parisi equation at large x.

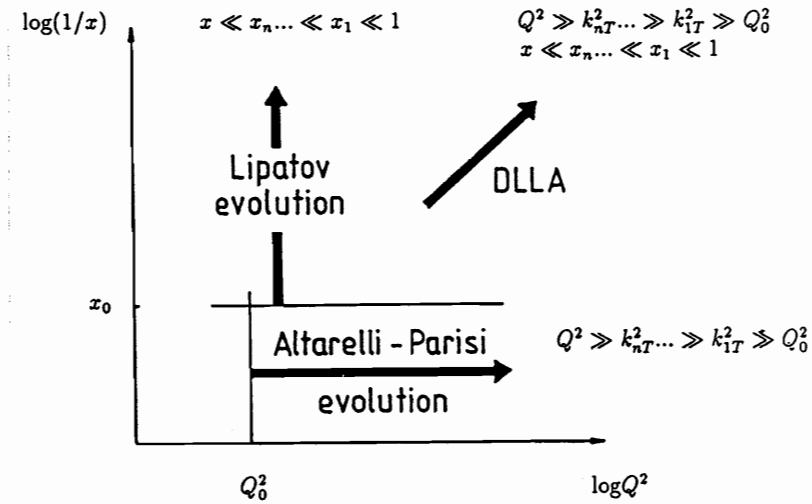

Figure 14: The three different limits of $g(x, Q^2)$ in the $\log Q^2$, $\log(1/x)$ plane: (i) the LL(Q^2) region where $\alpha_s \log Q^2 \sim 1$ but $\alpha_s \log(1/x)$ is small, reached by Altarelli-Parisi evolution from $g(x, Q_0^2)$, (ii) the DLL($Q^2, 1/x$) region where $\alpha_s \log Q^2 \log(1/x) \sim 1$ but $\alpha_s \log Q^2$ and $\alpha_s \log(1/x)$ are both small, and (iii) the LL($1/x$) limit where $\alpha_s \log(1/x) \sim 1$ but $\alpha_s \log Q^2$ is small, reached by evolution from $g(x_0, Q^2)$ using the Lipatov or BFKL equation. We also indicate the regions giving the dominant contributions in the integrations over the phase space of the emitted gluons; these are strongly-ordered in the longitudinal and/or transverse momenta of the gluons along the chain.

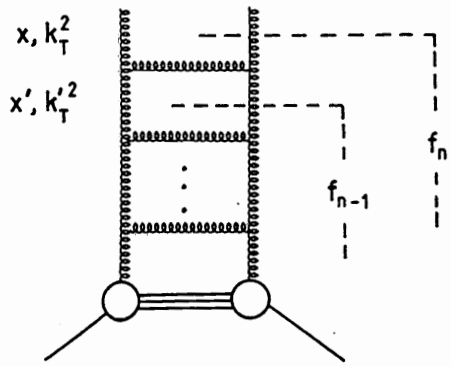

Figure 15: Diagrammatic representation of the BFKL recursion relation (70).

Balitsky [23]. It turns out that one set of diagrams, which must be included, can be shown to collectively reduce to the reggeization of the t-channel (i.e. "vertical") gluons in the ladder. If you are willing to take this ingenious LL$(1/x)$ summation of BFKL on trust, then the result may be written in the form of a recursion relation (see Fig. 15) which relates the n-rung contribution f_n to the $(n-1)$-rung contribution f_{n-1}

$$f_n(x,k_T^2) \;=\; \int_x^1 \frac{dx'}{x'} \int dk_T'^2\, K(k_T,k_T')\, f_{n-1}(x',k_T'^2), \tag{70}$$

where the BFKL or Lipatov kernel is

$$K(k_T,k_T') \;=\; \frac{3\alpha_s}{\pi} k_T^2 \left\{ \frac{1}{k_T'^2|k_T^2-k_T'^2|} - \beta(k_T^2)\delta(k_T^2-k_T'^2) \right\} \tag{71}$$

with

$$\beta(k_T^2) \;=\; \int \frac{dk_T'^2}{k_T'^2} \left\{ \frac{1}{|k_T^2-k_T'^2|} - \frac{1}{(4k_T'^4+k_T^4)^{\frac{1}{2}}} \right\}. \tag{72}$$

Here we work in terms of the *unintegrated* gluon distribution, $f(x,k_T^2)$, in which we unfold the "last" k_T^2 integration of the gluon distribution $g(x,Q^2)$ that we have been using hitherto;

$$xg(x,Q^2) \;=\; \int^{Q^2} \frac{dk_T^2}{k_T^2} f(x,k_T^2). \tag{73}$$

The two terms in (71) correspond to real gluon emission and virtual corrections respectively; the apparent singularity at $k_T^2 = k_T'^2$ cancels between these two contributions.

Let us check that we reproduce the DLL approximation if we constrain the k_T's to be strongly ordered, i.e. $k_T^2 \gg k_T'^2$. Then (71) becomes

$$K(k_T,k_T') \;=\; \frac{3\alpha_s}{\pi}\frac{1}{k_T'^2}. \tag{74}$$

In this case the recursion relation (70) effectively becomes

$$f_n \;\approx\; \frac{3\alpha_s}{\pi}\frac{1}{n}\log\left(\frac{1}{x}\right)\frac{1}{n}\log\left(\frac{k_T^2}{Q_0^2}\right) f_{n-1} \tag{75}$$

and, on summing over n, we reproduce (69).

The BFKL kernel, (71), is much more complicated than (74) and it is not so simple to find the small x behaviour arising from the summation of the LL$(1/x)$ terms. The result is found to be

$$f(x,k_T^2) \;\sim\; h(k_T^2)x^{-\lambda} \tag{76}$$

as $x \to 0$, where λ is the maximum "eigenvalue" of the kernel.

Insight into the $x^{-\lambda}$ form may be obtained from a toy model [6] in which it is assumed that the kernel has a factorized form

$$K(k_T,k_T') \;=\; u(k_T)v(k_T') \tag{77}$$

although of course, we see the BFKL kernel (71) has a more complicated structure. Substitution into the recursion relation (70) then gives

$$f_n(x,k_T^2) \;=\; u(k_T)\int_x^1 \frac{dk'}{x'} \int dk_T'^2 v(k_T') f_{n-1}(x',k_T'^2), \tag{78}$$

which itself is of factorizable form

$$f_n(x,k_T^2) \;=\; u(k_T)t_n(x). \tag{79}$$

Rewriting the recursion relation (78) in terms of t_n we obtain

$$t_n(x) \;=\; \lambda \int_x^1 \frac{dx'}{x'} t_{n-1}(x') \tag{80}$$

where

$$\lambda \;=\; \int_0^\infty dk_T^2 u(k_T)v(k_T). \tag{81}$$

The nested integrations of (80) give

$$t_n(x) \;\sim\; \frac{\lambda^n}{n!}\log\left(\frac{1}{x}\right), \tag{82}$$

which on summing over n generate the small x behaviour

$$f(x,k_T^2) \;\sim\; h(k_T^2)\exp\left(\lambda\log\frac{1}{x}\right) \;=\; h(k_T^2)x^{-\lambda}. \tag{83}$$

The exponent λ, defined in (81), can be seen to be a eigenvalue of the kernel, viz.,

$$K \otimes u \equiv \int u(k_T)v(k'_T)u(k'_T)dk'^2_T = \lambda u. \tag{84}$$

Clearly the maximum eigenvalue will dominate the small x behaviour of the gluon distribution f.

We can use the recursion relation (70) to write the BFKL equation in either differential or integral form. Symbolically (70) has the structure

$$f_n = K\hat{\otimes}f_{n-1} \qquad \text{where} \qquad f = \sum_{n=0} f_n \tag{85}$$

and where the $\hat{}$ indicates that there is an x, as well as an k_T^2, convolution. Performing the sum from the $n = 1$ term, the symbolic recursion relation gives

$$f - f_0 = K\hat{\otimes}f$$

or, to be explicit, the integral equation

$$f(x, k_T^2) = f_0(x, k_T^2) + \int_x^1 \frac{dx'}{x'} \int dk'^2_T K(k_T, k'_T) f(x', k'^2_T) \tag{86}$$

where f_0 is frequently called the driving term. Eq. (86) may be used to obtain the BFKL equation in differential form

$$\frac{\partial f(x, k_T^2)}{\partial \log(1/x)} = \int dk'^2_T K(k_T, k'_T) f(x', k'^2_T). \tag{87}$$

For fixed α_s the BFKL equation can be solved analytically. The solution is found to be

$$\frac{f(x, k_T^2)}{k_T^{\frac{1}{2}}} \sim \frac{(x/x_0)^{-\lambda}}{[2\pi\lambda''\log(x_0/x)]^{\frac{1}{2}}} \exp\left(\frac{-\log^2(k_T^2/\bar{k}_T^2)}{2\lambda''\log(x_0/x)}\right) \tag{88}$$

where

$$\lambda = \frac{3\alpha_s}{\pi} 4\log 2 \tag{89}$$

and $\lambda'' = (3\alpha_s/\pi)28\zeta(3)$ where the Riemann zeta function $\zeta(3) = 1.202$. We see the characteristic $x^{-\lambda}$ behaviour, modulated by a $(\log(1/x))^{-\frac{1}{2}}$ factor. If we insert a typical value of α_s into (89) then we find $\lambda \approx 0.5$. This is the origin of the input forms $xg, x\bar{q} \sim x^{-\frac{1}{2}}$ for small x that were used in the global analyes of section 3 (see (32)).

Formula (88) shows another characteristic feature of the solutions of the BFKL equation. Since there is no ordering in k_T there will be a "random walk" in k_T as we proceed along the chain and evolution to smaller x will be accompanied by a diffusion in k_T. Formula (88) displays explicitly the diffusion pattern, namely a Gaussian distribution in $\log(k_T^2)$ with a width which grows as $(\log(1/x))^{\frac{1}{2}}$ as x decreases. The

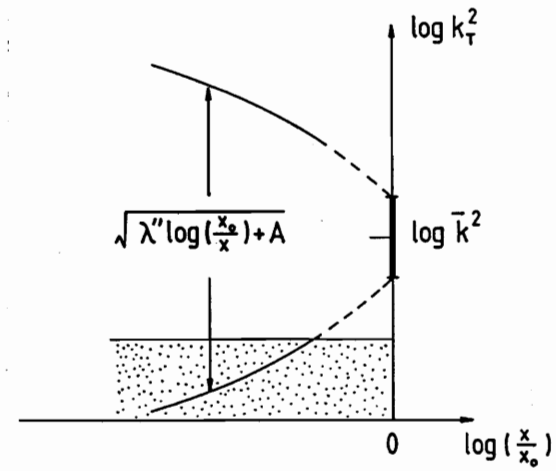

Figure 16: The variation in the width of the Gaussian $\log k_T^2$ distribution of $f(x, k_T^2)/(k_T^2)^{\frac{1}{2}}$ as we use the BFKL equation to evolve down in x from a starting distribution at $x = x_0$ of width $\sim \sqrt{A}$.

position of the maximum of the Gaussian distribution (given by $\log\bar{k}_T^2$), as well as the normalisation of the solution, is controlled by the boundary conditions at $x = x_0$, that is by $f(x_0, k_T^2)$.

The approximate analytic solution (88) only applies for $x \ll x_0$. For x near x_0 a more realistic treatment modifies the $\lambda''\log(x_0/x)$ factors in (88) to $\lambda''\log(x_0/x) + A$ where A depends on the initial k_T^2 distribution. Fig. 16 shows a sketch of the diffusion pattern. We foresee that diffusion will be a problem in the applicability of the BFKL equation since it can lead to an increasingly large contribution from the infrared (and ultraviolet) region of k_T^2 where the equation is not expected to be valid. We return to this discussion in section 8.

7. Shadowing and the GLR equation

The increase $f \sim x^{-\lambda}$ or $xg \sim x^{-\lambda}$, as x decreases, cannot go on indefinitely. If the density of gluons within the proton becomes too large they can no longer be treated as free partons. The growth, as $x \to 0$, must eventually be suppressed by gluon recombination. When do we expect the "shadowing" contributions to start to become appreciable? If we view the proton from a frame in which its momentum p is large, but in which $xp \gg Q$, then a measurement of $g(x, Q^2)$ probes a gluon of transverse size $\sim 1/Q$, but much smaller longitudinal size $\sim 1/px$, so that the proton

appears as a thin disc. The number of gluons, n_g, per unit of rapidity is $xg(x,Q^2)$ and the gluon-gluon cross section $\hat{\sigma} \sim \alpha_s(Q^2)/Q^2$, so the crucial parameter is

$$W \equiv \frac{n_g \hat{\sigma}}{\pi R^2} \sim \frac{\alpha_s(Q^2)}{\pi R^2 Q^2} xg(x,Q^2) \tag{90}$$

where R is the radius of the proton. In regions of x and Q^2 where $W \ll 1$ the interaction between the gluons should be negligible. However at sufficiently small x, when $W \sim \alpha_s$, we must allow for a suppression of the growth of the gluon density due to $2g \to g$ recombination. By carefully considering QCD diagrams which become important at small x, recombination was estimated some time ago by Gribov, Levin and Ryskin [25], and a little later by Mueller and Qiu [26]. To a first approximation the normal evolution, Fig. 17(a), is corrected by including Fig. 17(b) (the so-called "fan" diagram) in which the gluon ladder branches into two ladders which couple to the proton. The triple ladder vertex (shown as a rectangle) represents the sum of several (non-planar) diagrams. The iteration of this fan diagram produces a whole series of fan diagrams like the one shown in Fig. 17(c). In order to make progress GLR assumed that the coupling of n gluon ladders to the proton is proportional to the nth power of the single ladder coupling and in this way they were able to account for these shadowing effects by including an additional term in the BFKL equation, (87), so that

$$\frac{\partial f(x,k_T^2)}{\partial \log(1/x)} = K \otimes f - \frac{81\alpha_s^2(k_T^2)}{16R^2k_T^2}[xg(x,k_T^2)]^2. \tag{91}$$

The minus sign and the quadratic nature of the extra term reflect the suppression of growth of f, as x decreases, due to gluon recombination. The equation is known as the GLR equation [25]. The derivation of the GLR equation assumes that there are no correlations between the two gluon ladders (in Fig. 17(b)) which recombine. However Bartels [27], and subsequently Levin et al. [28], have established that there is a weak interaction ($\sim 1/N_c^4 \sim 10^{-2}$) between the ladders. The consequences of this additional interaction are the subject of debate [29].

The GLR equation includes only the leading $O(\alpha_s)$ shadowing corrections. If we were to proceed to ultra small x we would pass from the region where $W \lesssim O(\alpha_s)$ into the region where $W \gtrsim O(\alpha_s)$ where, first, higher-order shadowing effects became significant, but soon into a region where perturbative QCD is not applicable. We may thus only regard the GLR equation to be a reasonable approximation below a "critical line" which divides the (x,Q^2) domain into regions with $W \lesssim O(\alpha_s)$ from regions with $W \gtrsim O(\alpha_s)$, see Fig. 18. From (90) it is clear that as Q^2 increases shadowing becomes less important as Fig. 18 indicates.

Quantitatively the crucial "shadowing" parameter in (91) is R. It says how the gluons are concentrated within the proton. The conventional assumption is that they are uniformly spread across the proton; then R is the proton radius (~ 5 GeV^{-1}). However it has been advocated that they may be concentrated in "hot-spots" within the proton. Analyses have therefore also been performed with $R = 2$ GeV^{-1}. These

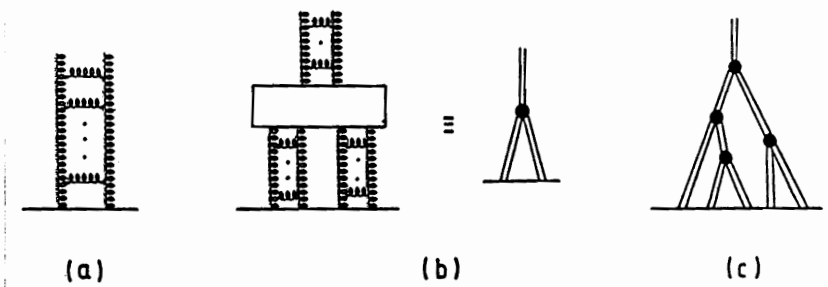

Figure 17: (a) The ladder diagram responsible for the BFKL "linear" QCD evolution (87), at small x; (b) the basic gluon shadowing or recombination diagram, also pictured as a "fan" diagram; (c) the sum of fan diagrams, such as the one shown, form the basis of the "quadratic" GLR equation, (91).

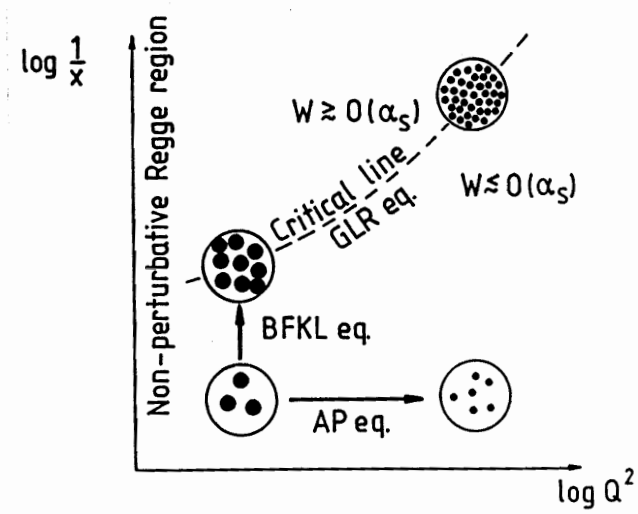

Figure 18: The (x,Q^2) regions of validity of the various evolution equations. The gluonic content of the proton (as resolved by a Q^2 probe) is also indicated. Perturbative QCD is applicable below the critical line (provided $Q^2 \gg \Lambda^2$).

numerical studies [6, 30, 31] of shadowing effects using (91) indicate that the kinematic regime accessible at HERA is below the critical line, unless very small "hot-spots" exist.

8. Solutions and applications of the BFKL equation

Recently there have been several studies of the properties of the solutions of the BFKL equation [30, 31, 32, 33, 34]. In some cases numerical solutions have been obtained. The usual technique is to solve the differential form of the equation, (87), by step-by-step integration down in x from an input distribution $f(x_0, k_T^2)$, at say $x_0 = 0.01$, determined from one of the parton sets of section 3. Running α_s and the effects of shadowing have been incorporated [30, 31]. One straightforward way to avoid the diffusion of the solution into the non-perturbative infrared region is to impose a lower limit cut-off k_0^2 on the $k_T'^2$ integration in (87). For a given value of k_T^2, the characteristic behaviour $f(x, k_T^2) \sim Cx^{-\lambda}$ soon sets in with decreasing x. The normalisation of the solution C is found to be much more sensitive to the choice of the cut-off k_0^2 than is the value of λ [34]. For $k_0^2 \simeq 1$ GeV^2 we find $\lambda \simeq 0.5$ essentially independent of the value of k_T^2.

The resummation of the gluon ladders, $f(x, k_T^2)$, is a universal ingredient in the perturbative QCD predictions of all small x processes driven by the gluon. For example $f(x, k_T^2)$ occurs in the calculation of the structure functions; of deep-inelastic events with jets; of heavy quark-pair[35], J/ψ and prompt photon production; as well as deep inelastic diffraction at small x.

(a) QCD predictions of deep inelastic structure functions at small x

At small x, say $x \sim 10^{-3}$, the deep inelastic probe dominantly interacts with a sea quark and so, to leading order, the structure functions $F_i(x, Q^2)$ reflect the small x behaviour of the sea quark distributions. Since the density of gluons increases rapidly with decreasing x the sea quark distributions are themselves increasingly dominated by the gluon distribution, via $g \to q\bar{q}$. This component may be calculated in perturbative QCD. The relevant diagram is shown in Fig. 19(a). According to the k_T-factorization [36] the contribution to the deep inelastic structure functions, say F_2^{ep}, may be written in the form [31]

$$F_2(x, Q^2) \;=\; \int_x^1 \frac{dx'}{x'} \int \frac{dk_T^2}{k_T^4} f\left(\frac{x}{x'}, k_T^2\right) F_2^{(0)}(x', k_T^2, Q^2) \qquad (92)$$

where x/x' is the longitudinal momentum fraction carried by the gluon which dissociates into the $q\bar{q}$ pair. The function $F_2^{(0)}$ can be calculated from the quark box (and crossed box) approximation to the photon-gluon subprocess shown in the upper part

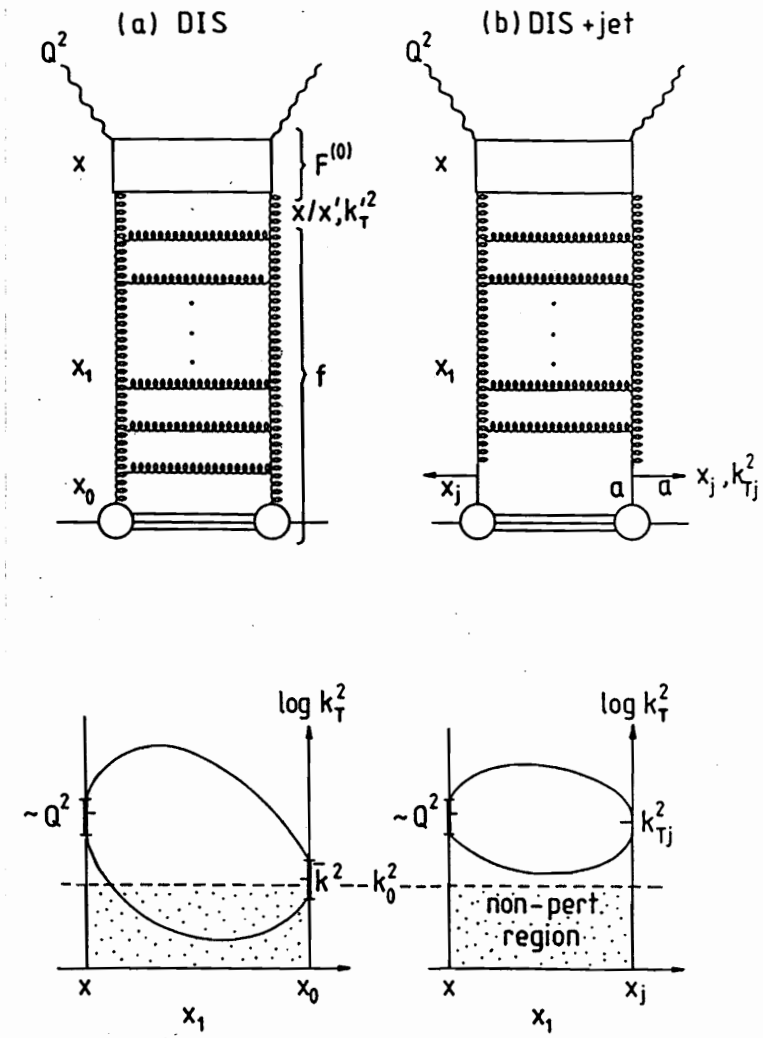

Figure 19: The upper diagrams show a gluon "ladder" contribution to small x for (a) deep-inelastic scattering and (b) for deep-inelastic scattering together with an energetic jet. The quark box factor $F^{(0)}$ implicitly includes the contribution of the crossed box. The lower sketches show the k_T^2 diffusion patterns in the form of the variation of the width of the log k_T^2 distributions of (93) as a function of x_1 along the chain.

of Fig. 19(a). We may regard $F^{(0)}$, or rather to be dimensionally correct $F^{(0)}/k_T^2$, as the structure function of a gluon of approximate virtuality k_T^2. The gluon density function f, which denotes the sum of the gluon "ladder" diagrams, is obtained by solving the BFKL equation.

The perturbative QCD predictions for F_2^{ep} [34] are compared with preliminary H1 data in Fig. 20. We see the normalisation is infrared cut-off dependent (with a "cut-off" value $k_a^2 = 1$ GeV^2 favoured) but that the shape is in excellent agreement with the data. The comparison suggests that HERA may have seen the first indication of the BFKL growth caused by the resummation of soft gluons.

Fig. 19 also shows the effects of diffusion in k_T^2. Unlike Fig. 16 the diffusion pattern is now determined by boundary conditions at both ends of the gluon ladder. To be specific it is given by [33, 34]

$$f(x_1, k_T^2) f_u\left(\frac{x}{x_1}, k_T^2\right)/k_T^2 \sim \frac{x^{-\lambda}}{\sqrt{\log(x_0/x_1)\log(x_1/x)}} \times$$

$$\times \exp\left(-\frac{\log^2(k_T^2/\bar{k}^2)}{2\lambda''\log(x_0/x_1)} - \frac{\log^2(k_T^2/\bar{k}_u^2)}{2\lambda''\log(x_1/x)}\right) \qquad (93)$$

where $\bar{k}_u^2$ is determined from boundary conditions controlled by the quark box function $F_2^{(0)}$. The variation of the width of the diffusion pattern (93), as x_1 varies between x and x_0, is sketched in the lower part of Fig. 19(a). Even for large Q^2, the boundary conditions at x_0 mean that the non-perturbative infrared region is penetrated, which is reflected in the cut-off dependence of the perturbative QCD predictions shown in Fig. 20.

(b) Deep inelastic events containing a measured jet

A major problem in identifying the characteristic BFKL $x^{-\lambda}$ behaviour from the observed shape of $F_2(x, Q^2)$ at small x is that the predictions depend on assuming a set of "starting" distributions, $f_a(x, Q^2)$, as a function of x at some $Q^2 = Q_0^2$. The necessity of this input is a reflection of our lack of knowledge of the non-perturbative regime. As a result, we cannot be certain whether the observed steep behaviour at $x \sim 10^{-3}$ is indeed a manifestation of the BFKL perturbative QCD effects or if it is due to the evolution from a steep non-perturbative input x distribution. Processes such as heavy quark pair, J/ψ and prompt photon production encounter the same dilemma.

However Mueller [37] has indicated an ingenious way to side-step the problem. The suggestion is to observe deep inelastic (x, Q^2) events which contain a measured jet (x_j, k_{Tj}^2) in the kinematic regime where (i) the transverse momentum of the jet satisfies $k_{Tj}^2 \simeq Q^2$, (ii) the jet longitudinal momentum, x_j, is as large as is experimentally feasible, and (iii) $z \equiv x/x_j$ is small. A diagrammatic representation of the process is shown in Fig. 19(b); since x_j is to be chosen as large as experiments allow ($x_j \sim$

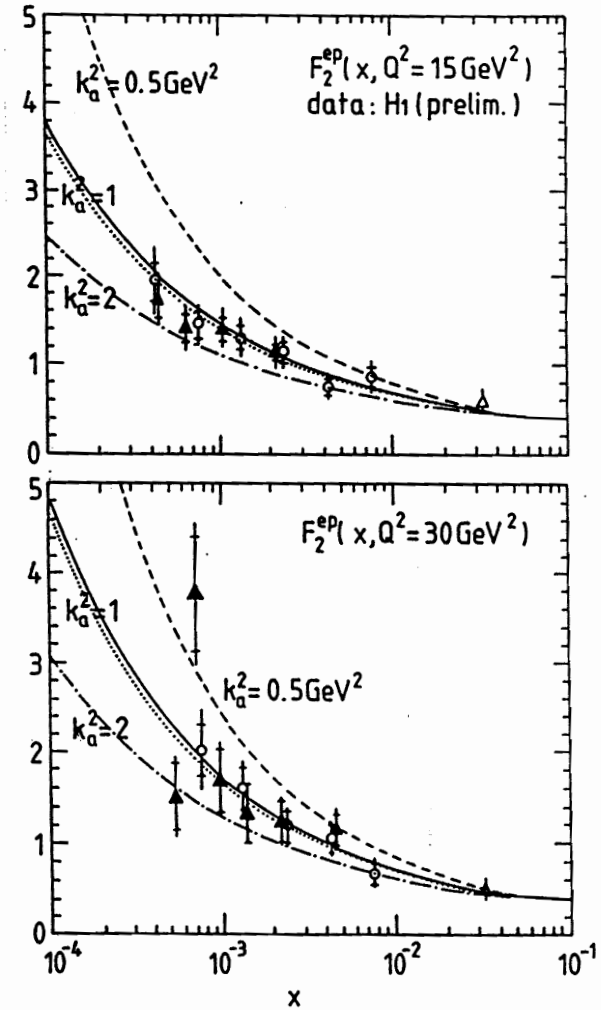

Figure 20: The perturbative QCD predictions for $F_2^{ep}(x, Q^2)$ obtained from the k_T-factorization formula, (92), for different choices of the infrared cut-off parameter k_a^2, compared with preliminary data obtained by the H1 collaboration [18] at HERA. The predicted curves contain a slowly varying "background" non-BFKL contribution estimated from the measured value of $F_2(x, Q^2)$ at $x = 0.1$. The figure is taken from ref. [34].

0.1) the strong ordering assumed at the parton a-gluon vertex should be a good approximation. The beauty of this measurement is that attention is focussed directly on the BFKL $z^{-\lambda}$-type behaviour at small z arising from the resummation of soft gluon emissions. The choice $k_{Tj}^2 \simeq Q^2$ neutralizes the ordinary gluon radiation which would have arisen from the Altarelli-Parisi evolution in Q^2.

It can be shown [38] that the differential structure function has a leading $z(\equiv x/x_j)$ form

$$x_j \frac{\partial F_2}{\partial x_j \partial k_{Tj}^2} \simeq \alpha_s(Q^2) \left[\sum_a x_j f_a(x_j, k_{Tj}^2) \right] z^{-\lambda}, \tag{94}$$

where $\sum f_a = g + \frac{4}{9}(q + \bar{q})$, which indeed contains the anticipated $z^{-\lambda}$ behaviour. As before, λ is the maximum eigenvalue of the BFKL kernel. The parton distributions $f_a(x_j, k_{Tj}^2)$ that are needed in (94) occur for x values where they are well measured and so, in principle, observation of the differential structure function should allow an unambiguous determination of λ.

Another advantage of this process is that we can choose $k_{Tj}^2 \approx Q^2$ sufficiently large to minimize the k_T diffusion into the infrared region; a choice which, incidentally, will also suppress the contamination from bremsstrahlung background jets. A typical diffusion pattern is shown in Fig. 19(b). As compared to the pattern in Fig. 19(a), we now have a $\delta(k_T^2 - k_{Tj}^2)$ distribution at the "bottom" of the gluon ladder.

9. Conclusions

Once more deep inelastic scattering has become a "hot" issue, stimulated by much new data[6] from fixed target and HERA experiments. We have seen that the former data now pin down the parton distributions rather precisely for $x \gtrsim 0.05$. Indeed the wide range of data that are well described in this way provide an impressive confirmation of QCD. With the new HERA data it is fair to say that small x physics has come of age. Novel perturbative QCD effects are expected in this regime and seem to be reproduced in the data. However we are a long way from having a deep understanding of the small x regime. From the perturbative viewpoint the higher order effects are far from under control. Attempts to approach the HERA regime from the non-perturbative or Regge domain have not been discussed in these lectures. Such studies present enormous, but worthwhile, challenges. Nevertheless from all points of view the new HERA data have already stimulated much theoretical activity, which will hopefully lead to a greater understanding of one of the most interesting areas of QCD.

[6] This year has also seen renewed interest in the spin structure of the nucleon with the recent polarised neutron deep inelastic measurements [39], to complement the earlier polarised proton experiments [40].

Acknowledgements

It is a pleasure to thank Fernando Barreiro and his colleagues, and the Universidad Autónoma de Madrid for their warm hospitality during the meeting. I also thank the other participants for numerous stimulating discussions. I am grateful to my collaborators Victor Fadin, Jan Kwiecinski, Dick Roberts and James Stirling from whom I have learnt so much about this topic.

References

[1] E. Reya, Phys. Rep. **69** (1981) 195.
G. Altarelli, Phys. Rep. **81** (1982) 1.
F.J. Yndurain, *QCD: an Introduction to the Theory of Quarks and Gluons*, Springer Verlag (1983).
M.R. Pennington, Rep. Prog. Phys. **46** (1984) 393.
V. Barger and R.J.N. Phillips, *Collider Physics*, Addison Wesley (1987).
T. Muta, *Foundations of QCD*, World Scientific (1987).
R.D. Field, *Applications of Perturbative QCD*, Addison Wesley (1989).
R.G. Roberts, *The Structure of the Proton*, Cambridge Univ. Press (1990).
Z. Kunszt, Proc. of Boulder Theoretical Advanced Study Institute, 1990, eds. M. Cvetić and P. Langacker, World Scientific, p.229.
R.K. Ellis and W.J. Stirling, Proc. 1988 CERN School of Physics, CERN Yellow Report 91-01, p.135.
Yu.L. Dokshitzer, V.A. Khoze, A.H. Mueller and S.I. Troyan, *Basics of Perturbative QCD*, Editions Frontieres (1991).
R.D. Peccei, Proc. 19th SLAC Summer Inst. in Particle Physics, SLAC Report 398 (1992) 259.

[2] F.E. Close, *An Introduction to Quarks and Partons*, Academic Press (1979).
F. Halzen and A.D. Martin, *Quarks and Leptons*, Wiley (1984).

[3] W.L. Van Neerven, these proceedings; see also E.B. Zijlstra, Univ. of Leiden thesis (1993).

[4] BCDMS collaboration: A.C. Benvenuti *et al.*, Phys. Lett. **223B** (1989) 485.

[5] NMC: P. Amaudruz *et al.*, Phys. Lett. **295B** (1992) 159.

[6] J. Kwiecinski, A.D. Martin, R.G. Roberts and W.J. Stirling, Phys. Rev. D**42** (1990) 3645.

[7] A.D. Martin, W.J. Stirling and R.G. Roberts, Phys. Rev. D **47** (1993) 867.

[8] A.D. Martin R.G. Roberts and W.J. Stirling, Phys. Rev. D**37** (1988) 1161; see also Phys. Lett. **206B** (1988) 327; Mod. Phys. Lett. A**4** (1989) 1135.
M. Diemoz, F. Ferroni, E. Longo and G. Martinelli, Z. Phys. C **39** (1988) 21.
P. Aurenche, R. Baier, M. Fontannaz, J.F. Owens and M. Werlen, Phys. Rev. D **39** (1989) 3275.

[9] A.D. Martin, W.J. Stirling and R.G. Roberts, Phys. Lett. B **306** (1993) 145.

[10] CTEQ collaboration: J. Botts, J. Morfin, J. Owens, J. Qiu, W.-K. Tung and H. Weerts, Phys. Lett. **304B** 1993) 159.

[11] CCFR collaboration, Phys. Rev. Lett., to be published.

[12] WA70 collaboration, M. Bonesini *et al.*, Z. Phys. C**38** (1988) 371.

[13] A.D. Martin, W.J. Stirling and R.G. Roberts, Proc. of Workshop on "HERA: a new frontier of QCD", Durham, March 1993, J. Phys. G (in press).

[14] C. Foudas *et al.*, Phys. Rev. Lett. **64** (1990) 1207.
S.A. Rabinowitz *et al.*, Phys. Rev. Lett. **70** (1993) 134.

[15] NMC collaboration, P. Amaudruz *et al.*, Phys. Rev. Lett. **66** (1991) 2712.

[16] NMC: E.M. Kabuß, Nucl. Phys. B (Proc. Suppl.) **29A** (1992) 1.

[17] A.D. Martin, W.J. Stirling and R.G. Roberts, Phys. Lett. B**308** (1993) 377.

[18] A. De Roeck, Proc. of the Workshop on " HERA: a new frontier for QCD", Durham, March 1993, J. Phys. G (in press);
M.W. Krasny, these proceedings.

[19] L.V. Gribov, E.M. Levin and M.G. Ryskin, Phys. Rep. **100** (1983) 1.
J. Bartels, Particle World **2** (1991) 46.
E.M. Levin, Orsay Lectures, LPTHE 91/02 (1991).
A.D. Martin, Acta Physica Polonica B**22** (1991) 1095.
E.M Levin, Proc. of Conf. on " QCD – 20 Years later", Aachen, June (1992).
Proc. of the Workshop on "Physics at HERA", eds. W. Buchmüller and G. Ingelman, DESY, Hamburg, Oct. 1991, vols 1-3.
B. Badelek, K. Charchula, M. Krawczyk and J. Kwiecinski, Rev. Mod. Phys. 64 (1992) 927.

J. Kwiecinski, Proc. of 32nd Schladming School, Austria, March (1993).
Proc. of the Workshop on "HERA: a new frontier for QCD", Durham, March 1993, J. Phys. G (in press).

[20] M. Glück, E. Reya and A. Vogt, Phys. Lett. B**306** (1993) 391.

[21] M. Fontannaz, these proceedings.

[22] Yu.L. Dokshitzer, Sov. Phys. JETP **46** (1977) 641.

[23] E.A. Kuraev, L.N. Lipatov and V. Fadin, Zh. Eksp. Teor. Fiz. **72** (1977) 373; Sov. Phys. JETP **45** (1977) 199.
Ya.Ya. Balitskij and L.N. Lipatov, Yad. Fiz. **28** (1978) 1597; Sov. J. Nucl. Phys. **28** (1978) 822.
L.N. Lipatov, in *Perturbative QCD*, ed. A.H. Mueller (World Scientific, Singapore, 1989) p.411.
J.B. Bronzan and R.L. Sugar, Phys. Rev. D**17** (1978) 585.
T. Jaroszewicz, Acta Phys. Polon. B**11** (1980) 965.

[24] M. Ciafaloni, Nucl. Phys. **296** (1988) 49.
S. Catani, F. Fiorani and G. Marchesini, Phys. Lett. B**234** (1990) 339; Nucl. Phys. B**336** (1990) 18.
G. Marchesini, Proc. of Workshop " QCD at 200 TeV", Erice, Italy, June 1990, eds. L. Cifarelli and Yu.L. Dokshitzer, Plenum Press, New York 1992, p.183.

[25] L.V. Gribov, E.M. Levin and M.G. Ryskin, Phys. Rep. **100** (1983) 1.

[26] A.H. Mueller and J. Qiu, Nucl. Phys. B**268** (1986) 427.

[27] J. Bartels, Phys. Lett. B**298** (1993) 204; DESY preprint, DESY 93-028.

[28] E.M. Levin, M.G. Ryskin and A.G. Shuvaev, Nucl. Phys. B**387** (1992) 589.

[29] Proc. of the Workshop on " HERA: a new frontier for QCD", Durham, March 1993, J. Phys. G (in press).

[30] J. Kwiecinski, A.D. Martin and P.J. Sutton, Phys. Rev. D**44** (1991) 260; Phys. Lett. B**264** (1991) 199.

[31] A.J. Askew, J. Kwiecinski, A.D. Martin and P.J. Sutton, Phys. Rev. D**47** (1993) 3775.

[32] E.M. Levin, G. Marchesini, M.G. Ryskin and B.R. Webber, Nucl. Phys. B**357** (1991) 167.
J.R. Forshaw and P.N. Harriman, Phys. Rev. D**46** (1992) 3778.
J.C. Collins and P.V. Landshoff, Phys. Lett. **276B** (1992) 196.
R.E. Hancock and D.A. Ross, Nucl. Phys. B**383** (1992) 575.

J.R. Forshaw, P.N. Harriman and P.J. Sutton, Manchester preprint M/C-TH 93/14 (1993).

[33] J. Bartels and H. Lotter, Phys. Lett. **B309** (1993) 400.

[34] A.J. Askew, J. Kwiecinski, A.D. Martin and P.J. Sutton, Durham preprint DTP/93/38 (1993), and preprint in preparation.

[35] see, for example, A. Ali, these proceedings.

[36] S. Catani, M. Ciafaloni and F. Hautmann, Phys. Lett. **242B** (1990) 91; Nucl. Phys. **B366** (1991) 135.
S. Catani, M. Ciafaloni and F. Hautmann, Proc. of the Workshop " Physics at HERA", DESY, Hamburg, Germany, October 1992, eds. W. Buchmüller and G. Ingelman, Vol. 2 (1992) p.690.

[37] A.H. Mueller, Nucl. Phys. B(Proc. Suppl.) **18C** (1990) 125; J. Phys. **G17** (1991) 1443.

[38] J. Bartels, A. De Roeck and M. Loewe, Z. Phys. **C54** (1992) 635; Nucl. Phys. B (Proc. Suppl.) **29A** (1992) 61.
W.-K. Tang, Phys. Lett. **278B** (1992) 363.
J. Kwiecinski, A.D. Martin and P.J. Sutton, Phys. Rev. **D46** (1992) 921; Phys. Lett. **287B** (1992) 254; Nucl. Phys. B (Proc. Suppl.) **29A** (1992) 67.

[39] SMC: B. Adeva *et al.*, Phys. Lett. **B302** (1993) 533.
E142 collaboration: P.L. Anthony *et al.*, Phys. Rev. Lett. **71** (1993) 959.

[40] J. Ashman *et al.*, Phys. Lett. **206B** (1988) 364; Nucl. Phys. **B328** (1989) 1.